Interstellar Ti II in the Milky Way and Magellanic Clouds[★]

Daniel E. Welty[1]†‡ and Paul A. Crowther[2]‡

[1]*Department of Astronomy, University of Illinois at Urbana/Champaign, 1002 W. Green St., Urbana, IL 61801, USA*
[2]*Department of Physics and Astronomy, University of Sheffield, Hicks Building, Hounsfield Rd., Sheffield 53 7RH*

ABSTRACT

We discuss several sets of Ti II absorption-line data, which probe a variety of interstellar environments in our Galaxy and in the Magellanic Clouds. Comparisons of high-resolution [full width at half-maximum (FWHM) $\sim$ 1.3–1.5 km s^{-1}] Ti II spectra of Galactic targets with corresponding high-resolution spectra of Na I, K I and Ca II reveal both similarities and differences in the detailed structure of the absorption-line profiles – reflecting component-to-component differences in the ionization and depletion behaviour of those species. Moderate-resolution (FWHM $\sim$ 3.4–4.5 km s^{-1}) spectra of more heavily reddened Galactic stars provide more extensive information on the titanium depletion in colder, denser clouds – where more than 99.9 per cent of the Ti may be in the dust phase. Moderate-resolution (FWHM $\sim$ 4.5–8.7 km s^{-1}) spectra of stars in the Magellanic Clouds suggest that the titanium depletion is generally much less severe in the Large and Small Magellanic Clouds than in our Galaxy [for a given $N(H_{tot})$, $E(B - V)$, or molecular fraction $f(H_2)$] – providing additional evidence for differences in depletion patterns in those two lower-metallicity galaxies. We briefly discuss possible implications of these results for the interpretation of gas-phase abundances in quasi-stellar object absorption-line systems and of variations in the D/H ratio in the local Galactic interstellar medium.

Key words: ISM: abundances – ISM: lines and bands – galaxies: ISM – Magellanic Clouds.

1 INTRODUCTION

Singly ionized titanium is unique among the small number of atomic species whose interstellar absorption features can be observed from the ground, in that its ionization potential is nearly coincident with that of neutral hydrogen – so that Ti II is a dominant ion in H I regions, with negligible contributions from ionized (H II) gas. The column density ratio $N(Ti II)/N(H_{tot})$ – where H_{tot} includes both neutral atomic and molecular hydrogen – thus gives a direct measure of the gas phase interstellar abundance of titanium. In principle, it is also fairly straightforward to obtain accurate column densities for Ti II. Several lines of Ti II, with a range in strength, are available between 3060 and 3390 Å – so that any effects of saturation in the

strongest line at 3383 Å may be estimated. Blending with stellar Ti II absorption features is not an issue for spectral types earlier than about B7 (Hobbs 1984).

The earliest surveys of Ti II absorption in the relatively nearby Galactic interstellar medium (ISM) indicated that even the λ3383 line is often fairly weak, and that the gas-phase titanium abundance is significantly sub-solar in most sight lines (Wallerstein & Goldsmith 1974; Stokes 1978). Most of the titanium in the Galactic ISM appears to be depleted into dust grains, with less than 1 per cent of the total (assumed solar) titanium in the gas in many sight lines. The $N(Ti II)/N(H_{tot})$ ratio thus appears to be an excellent indicator of the overall level of depletion in a given line of sight – at least in the local Galactic ISM (e.g. Jenkins 2004; Jenkins 2009). Because the Ti II lines are both weak (typically) and located in the near-UV, most subsequent surveys of interstellar Ti II have been undertaken at moderate spectral resolution (3–6 km s^{-1}) towards relatively bright and generally lightly reddened background target stars (Albert 1983; Albert et al. 1993; Welsh et al. 1997); some more reddened targets are included in the recent survey by Hunter et al. (2006).

Comparisons of the absorption-line profiles and column densities of Ti II with those of Na I and Ca II and examination of correlations with distance (to the target stars) have suggested that Ti II is distributed more similarly to Ca II, with both species primarily tracing the warmer, more smoothly distributed, more diffuse neutral component of the ISM (Edgar & Savage 1989; Crinklaw, Federman &

Joseph 1994). Overall, the ratio $N(\text{Ti\,\textsc{ii}})/N(\text{Ca\,\textsc{ii}})$ appears to be relatively constant, with a value of 0.3–0.4 (Albert 1983; Hunter et al. 2006), even though both Ti and Ca can exhibit wide variations in depletion and even though Ca\,\textsc{ii} can be either a dominant or a trace species in predominantly neutral regions. The distributions of both Ti\,\textsc{ii} and Ca\,\textsc{ii} are characterized by scale heights greater than 1000 pc perpendicular to the Galactic disc – significantly larger than the roughly 200 pc scale height of H\,\textsc{i} (Albert 1983; Edgar & Savage 1989; Albert et al. 1993; Albert, Welsh & Danly 1994; Lipman & Pettini 1995). Titanium is thus less severely depleted, by a factor of order 4, in the low Galactic halo at $250 \lesssim |z| \lesssim 1000$ pc, and is further enhanced in the gas phase in components at higher local standard of rest (LSR) velocities (Albert 1983).

Given the potential utility of Ti\,\textsc{ii} as a depletion indicator, observations of Ti\,\textsc{ii} have been employed in recent studies ranging from attempts to understand variations in the D/H ratio in the local ISM to interpretations of the gas phase abundances in QSO absorption-line systems. One possible explanation for the local variations in D/H is that deuterium could be preferentially depleted into dust grains (Jura 1982; Tielens 1983; Draine 2006), in which case one would expect correlations between D/H and the depletions of various refractory elements, such as Ti (Prochaska, Tripp & Howk 2005; Ellison, Prochaska & Lopez 2007; Lallement, Hébrard & Welsh 2008) or Si and Fe (Linsky et al. 2006). While there does appear to be a correlation between the titanium depletion $\delta(\text{Ti})$ and D/H, the correlation is not as strong and the slope of the relationship is not as steep as might have been expected from the analogous relations seen for $\delta(\text{Si})$ and $\delta(\text{Fe})$ (Ellison et al. 2007). Component-to-component differences between the depletions of Ti and D (Prochaska et al. 2005) may be a factor.

The gas phase abundances found for quasi-stellar object (QSO) absorption-line systems must reflect both the nucleosynthetic history of the absorbers (e.g. the relative contributions of Type I and Type II supernovae in enriching the ISM) and any (selective) depletion of various elements into dust – but disentangling the effects of those two factors is often difficult (e.g. Lauroesch et al. 1996; Lu et al. 1996; Prochaska & Wolfe 2002; Vladilo 2002; Dessauges-Zavadsky et al. 2004). In principle, comparisons between Ti\,\textsc{ii} and Fe\,\textsc{ii} may help to separate the two effects, as Ti (an α-element) is overabundant, relative to Fe and solar abundance ratios, in Galactic metal-poor stars, but is typically more severely depleted than Fe in the Galactic ISM (e.g. Dessauges-Zavadsky, Prochaska & D'Odorico 2002; Ledoux, Bergeron & Petitjean 2002). A supersolar Ti/Fe ratio in a QSO absorber would thus seem to imply that more massive stars (and associated Type II SNe) have dominated the heavy element enrichment of that system (and that the effects of depletion are minimal) – if the depletion patterns in low-metallicity systems are similar to those found in our Galaxy.

While the existing surveys of Ti\,\textsc{ii} absorption have provided a general picture of the behaviour of titanium in the Galactic ISM, there are several aspects that remain poorly understood. The moderate spectral resolution of most of the existing Ti\,\textsc{ii} data generally has not allowed detailed investigations of the properties of the individual interstellar components discerned in higher resolution spectra of Na\,\textsc{i}, K\,\textsc{i} and Ca\,\textsc{ii} (e.g. Welty, Hobbs & Kulkarni 1994; Welty, Morton & Hobbs 1996; Welty & Hobbs 2001; Price et al. 2001), which reveal variations in component properties (e.g. line widths, relative abundances) on velocity scales of $1–2\,\text{km s}^{-1}$. Moreover, while titanium is known to be severely depleted in some moderately reddened sight lines containing diffuse molecular material, little is known about the depletion behaviour of titanium in more heavily reddened sight lines (which may include some denser gas).

Significantly enhanced depletions were not found for iron in several recent samples of translucent sight lines (Snow, Rachford & Figoski 2002; Jensen & Snow 2007; Miller et al. 2007), but enhanced depletions in individual dense components could have been masked by contributions from more diffuse gas in the relatively low-resolution *FUSE* spectra [full width at half-maximum (FWHM) $\sim 20\,\text{km s}^{-1}$] used in the first two studies.

Very little is known regarding the depletion behaviour of titanium (and other elements) in lower metallicity systems. For example, Ti\,\textsc{ii} column densities have been reported for only a few sight lines in the Large and Small Magellanic Clouds (LMC/SMC; Caulet & Newell 1996; Welty et al. 1999a, 2001; Cox et al. 2006, 2007), where the current metallicities are typically 0.5 and 0.2 times solar, respectively (e.g. Russell & Dopita 1992; various references in the appendices in Welty et al. 1997, 1999a). The relatively nearby Magellanic Clouds provide an important venue for studies of the interstellar abundance/depletion patterns in low-metallicity galaxies, because the total interstellar (gas plus dust) abundances of many elements may be inferred from analyses of the abundances in stellar atmospheres and gaseous nebulae. Studies of the interstellar abundances in a small number of sight lines have revealed possible differences in depletion behaviour for Mg, Si and Ti (versus Fe and Ni) in at least some components in the LMC and SMC (Welty et al. 1997, 1999a, 2001, 2004, in preparation; see also Sofia et al. 2006).

In this paper, we present several sets of Ti\,\textsc{ii} absorption-line data, in order to further explore the behaviour of Ti\,\textsc{ii} in different interstellar environments: (1) high-resolution (FWHM $= 1.3–1.5\,\text{km s}^{-1}$) spectra of 17 relatively bright, lightly reddened Galactic stars – to enable detailed comparisons with corresponding high-resolution spectra of Na\,\textsc{i}, K\,\textsc{i}, Ca\,\textsc{i} and Ca\,\textsc{ii} – and thus estimation of the properties of individual components in those sight lines; (2) moderate resolution (FWHM $= 3.4–4.5\,\text{km s}^{-1}$) spectra of a number of fainter, more heavily reddened Galactic stars – to investigate the depletion behaviour of Ti in denser gas; and (3) moderate resolution (FWHM $= 4.5–8.7\,\text{km s}^{-1}$) spectra of 43 stars in the Magellanic Clouds – to examine the depletion behaviour of titanium in lower metallicity gas – to aid in understanding the Ti\,\textsc{ii} abundances in even lower metallicity absorption-line systems seen towards distant QSOs and gamma-ray bursts. These data thus include both the highest resolution Ti\,\textsc{ii} spectra available for the Galactic ISM and the most extensive Ti\,\textsc{ii} spectra available for the ISM in the Magellanic Clouds.

The following sections describe the various observational data (stellar samples, spectra, data reduction and analysis procedures), the derived Ti\,\textsc{ii} column densities and titanium abundances (compared with similar data for other species), and the implications of those data for understanding the properties of interstellar clouds in various environments. Several appendices contain plots of all the observed Ti\,\textsc{ii} line profiles, lists of the individual component column densities derived from the highest resolution spectra, and two compilations of Ti\,\textsc{ii} equivalent widths and column densities (from both current and previous work) used in exploring possible correlations between Ti\,\textsc{ii} and other species.

2 DATA

The spectroscopic data collected in this survey were obtained using either the Kitt Peak 0.9-m coudé feed telescope and echelle spectrograph or the ESO/VLT UT2 telescope and UVES spectrograph (Dekker et al. 2000). The various observing runs are summarized in Table 1, where we list for each run the telescope, spectrograph,

Table 1. Observing Runs.

Date	Facility	Resolution (km s^{-1})	Galactic	SMC	LMC	Run
1994 Sep	KPNO/coudé feed (cam 6)	1.3	11	0	0	K94
1995 Apr	KPNO/coudé feed (cam 6)	1.5	13	0	0	K95
2000 Jun-Jul	ESO/VLT (UT2) + UVES	3.8	29	0	0	V00
2000 Nov	KPNO/coudé feed (cam 5)	3.4	9	0	0	K00
2001 Sep	ESO/VLT (UT2) + UVES	5.0	0	1	0	V01
2002 Nov-Dec	ESO/VLT (UT2) + UVES	8.7	0	3	10	V02
2003 Nov	ESO/VLT (UT2) + UVES	4.5	7	5	7	V03
2004 Nov-Dec	ESO/VLT (UT2) + UVES	8.7	0	6	12	V04

V00 data are from programme 65.I-0526 (E. Roueff, PI); V01 data are from programme 67.C-0281 (P. Ehrenfreund, PI).

resolution, number of sight lines and a three-character code used to identify data from the run in other tables and figures.

2.1 Stellar sample

Tables 2–4 list the 60 Galactic (MW), 15 SMC and 28 LMC sight lines for which spectra are included in this survey. For each sight-line, the tables give Galactic (MW) or equatorial coordinates (MC), spectral type, V, $E(B - V)$ (both total and MC), either stellar distance (MW) or radial velocity (MC), and the observing run(s) in which the observations were obtained. The sightlines are ordered by right ascension in each table.

The Milky Way targets range from very nearby, unreddened stars to distant, heavily reddened stars; nearly all the sight lines primarily probe gas within the Galactic disc. The sample is not unbiased – in that it includes both stars observed in previous high-resolution surveys of Na I, K I and/or Ca II (Welty et al. 1994, 1996; Welty & Hobbs 2001), stars observed in an ongoing survey of the diffuse interstellar bands (Thorburn et al. 2003), and a number of more reddened stars – but the set of sight lines does explore a variety of regions and environments within the local Galactic ISM. Many of the spectral types and photometric data were taken from Thorburn et al. (2003); the rest were derived from values listed in the SIMBAD data base. Most of the targets are O or early-B stars, but there are a few late-B and A stars included as well. Fifteen of the 60 stars are lightly reddened, with $E(B - V) < 0.10$; 29 others have $E(B - V) \geq 0.35$. Stellar distances were taken from Thorburn et al. (2003) or Snow, Destree & Welty (2008; for Sco-Oph) or were estimated from the spectral types and photometry, using the absolute magnitudes of Blaauw (1963) and the intrinsic colours of Johnson (1963) and assuming total visual extinctions of $3.1 \times E(B - V)$. Sixteen of the stars are within 200 pc of the Sun; 11 are at distances ≥ 1000 pc; only one (ρ Leo) lies more than 200 pc from the Galactic plane.

The sample of Magellanic Clouds sight lines also is not unbiased. Most of the 43 stars were observed primarily for studies of stellar properties at lower metallicities (e.g. Crowther et al. 2002; Evans et al. 2004); 13 stars, with typically higher $E(B - V)$ and known strong absorption from interstellar Na I and/or H_2, were observed in a search for interstellar molecular absorption lines (Welty et al. 2006). All of the SMC and LMC targets are O, early B, or Wolf–Rayet stars, with $11.0 \lesssim V \lesssim 14.6$; some appear to be unresolved binary (or multiple) systems. The stellar coordinates are from the catalogues painstakingly compiled by B. Skiff.[1] Refer-

ences for the spectral types, V magnitudes, and $B - V$ colours for the stars are given in footnotes to Tables 3 and 4. In general, we preferred the CCD photometry of Massey (2002) and Parker (1993), which should better account for blending, near neighbours and local fluctuations in the background than the earlier studies based on aperture photometry. In most cases, the total $E(B - V)$ colour excesses (first entries) were obtained using the intrinsic colours of FitzGerald (1970) or Walborn et al. (2002a); for the few Wolf–Rayet stars, the intrinsic colours were estimated from theoretical spectral energy distributions (e.g. Crowther 2007). Only two SMC and six LMC sight lines have total $E(B - V)$ greater than 0.2 mag. For the Galactic contributions to those total $E(B - V)$, we adopted a constant 0.04 mag for all the SMC sight lines (Schlegel, Finkbeiner & Davis 1998) and values ranging from 0.02 to 0.09 mag for the LMC sight lines [estimated from fig. 13 of Staveley-Smith et al. (2003)]. The second $E(B - V)$ entries give the corresponding contributions for the SMC or LMC ISM (total minus Galactic). Considering that the uncertainties in the photometry, in the spectral types and intrinsic colours and in the Galactic contribution to the colour excess could each be several hundredths of a magnitude, it is notable that $E(B - V)_{MC}$ is not less than zero for any of the 43 sight lines.

Where possible, two stellar radial velocities are listed for the Magellanic Clouds targets. The first value is from the literature, with references in footnotes to the tables. Many of those values were derived from objective prism spectra, and have an estimated accuracy of order 15 km s^{-1} (e.g. Fehrenbach & Duflot 1982). The second value is estimated from the spectra analyzed in this paper, using the stellar H I lines; the He I lines near 3926.5, 3964.7 and 5875.6 Å (in air); and/or the Ca II lines near 3933.7 and 3968.5 Å. In most cases, the two values agree within ± 20 km s^{-1}.

2.2 Observations and data processing

2.2.1 KPNO coudé feed

High-resolution spectra of 17 relatively bright ($V \lesssim 4.7$) Galactic stars were obtained with the 0.9-m KPNO coudé feed telescope and echelle spectrograph during two runs in 1994 (K94) and 1995 (K95). Both runs employed set-ups similar to those used in previous high-resolution surveys of K I, Ca I and Ca II (Welty, Morton & Hobbs 1996; Welty, Hobbs & Morton 2003; Welty & Hobbs 2001) – with camera 6, grism 780-2 and the 3° wedge for cross-dispersion, and BG3+CuSO$_4$ filters to isolate the spectral region from about 3270 to 3490 Å. The set-ups used a very narrow slit, corresponding to about 0.65 arcsec on the sky, to achieve resolutions of 1.3–1.5 km s^{-1} (similar to the values achieved in the previous high-resolution surveys), as determined from the widths of the thorium lines in the

[1] ftp.lowell.edu/pub/bas/starcats

Table 2. Galactic Sight lines.

HD	Name	l (°′)	b (°′)	V	$E(B-V)$	Type	d (pc)	Runs
23180	o Per	160 22	−17 44	3.83	0.31	B1 III	280	K00
24398	ζ Per	162 17	−16 42	2.85	0.31	B1 Ib	300	K00
24534	X Per	163 05	−17 08	6.10	0.59	O9.5pe	590	K00
24760	ε Per	157 21	−10 06	2.89	0.10	B0.5V+A2	165	K94
27778	62 Tau	172 46	−17 23	6.36	0.37	B3 V	225	K00
32630	η Aur	165 21	00 16	3.17	0.02	B3 V	67	K95
35149	23 Ori	199 19	−17 52	5.00	0.11	B1 V	295	K00,V03
36486	δ Ori	203 51	−17 45	2.23	0.08	B0III+O9V	280	K94,K95
37022	θ¹ OriC	209 01	−19 23	5.13	0.34	O6-7p	450	K00
37043	ι Ori	209 32	−19 36	2.77	0.07	O9 III	450	K95
37128	ε Ori	205 13	−17 15	1.70	0.05	B0 Iae	350	K94
37742	ζ Ori A	206 27	−16 36	2.05	0.06	O9.5 Ibe	370	K94,K95
47839	15 Mon A	202 56	02 11	4.66	0.07	O7 Ve	950	K94,K95
	Walker 67	202 59	02 04	10.79	0.86	B2 V	950	V03
62542		255 55	−09 14	8.04	0.35	B5 V	246	V03
72127A		262 34	−03 22	5.20	0.10	B2 III	480	V03
72127B		262 34	−03 22	7.09	0.10	B2.5 V	480	V03
73882		260 11	00 38	7.22	0.70	O8 V	1100	V03
91316	ρ Leo	234 53	52 46	3.85	0.05	B1 Ib	760	K95
106625	γ Crv	290 59	44 30	2.59	0.00	B8 III	51	V00
110432		301 58	−00 12	5.31	0.51	B2pe	300	V00
112244		303 33	06 02	5.32	0.30	O9 Ibe	1250	V00
113904	θ Mus	304 40	−02 29	5.51	0.25	WC6+O6-7V	2200	V00
114213		305 11	01 19	8.97	1.12	B1 Ib	1700	V00
116658	α Vir	316 07	50 50	0.98	0.03	B1 III	80	K95
141637	1 Sco	346 06	21 43	4.64	0.15	B3 V	152	K95
143018	π Sco	347 12	20 14	2.89	0.04	B1V+B2V	180	K94,K95
144217	β¹ Sco	353 11	23 36	2.62	0.19	B1 V	124	K94,K95
147165	σ Sco	351 19	17 00	2.89	0.41	B2III+O9V	214	K95
147701		352 15	16 51	8.35	0.74	B5 III	153	V00
147888	ρ Oph D	353 39	17 43	6.74	0.47	B5 V	125	V00
147889		352 52	17 02	7.90	1.07	B2 V	118	V00
147933	ρ Oph A	353 41	17 41	5.02	0.48	B2 IV	111	V00
148184	χ Oph	357 56	20 41	4.42	0.52	B2 IVpe	161	V00
148379		337 15	01 35	5.36	0.72	B2 Iab	770	V00
149404		340 32	03 01	5.47	0.68	O9 Iae	820	V00
149757	ζ Oph	6 17	23 36	2.56	0.32	O9.5 V	140	K94,K95,V00
150136		336 43	−01 34	5.60	0.48	O6 III	1270	V00
152236	ζ¹ Sco	343 02	00 52	4.73	0.68	B1 Ia⁺pe	1800	V00
154368		349 58	03 13	6.13	0.78	O9 Ia	960	V00
159561	α Oph	35 54	22 35	2.08	0.00	A5 III	14	K94,K95
161056		18 41	11 47	6.30	0.62	B1.5 V	310	V00
166734		18 55	03 38	8.41	1.39	O8e	720	V00
167971		18 15	01 41	7.45	1.08	O8e	730	V00
	BD−14 5037	16 56	−00 57	8.24	1.55	B1.5 Ia	1100	V00
169454		17 32	−00 40	6.61	1.12	B1.5 Ia	930	V00
170740		21 04	−00 32	5.72	0.48	B2 V	213	V00
172028		31 03	02 50	7.83	0.79	B2 V	380	V00
182985		02 48	−22 38	7.47	0.12	A0 V	186	V00
183143		53 14	00 38	6.86	1.27	B7 Iae	1000	V00
188220		25 16	−20 59	8.04	0.27	A0 V	200	V00
197345	α Cyg	84 17	02 00	1.25	0.09	A2 Ia	540	K94
199579		85 42	−00 18	5.96	0.37	O6 Ve	1200	K00
205637	ε Cap	31 56	−44 59	4.65	0.02	B3 V:p	203	V00
206267		99 17	03 44	5.62	0.53	O6f	810	K00
207198		103 08	06 59	5.95	0.62	O9 IIe	1000	K00
210121		56 53	−44 28	7.67	0.40	B3 V	210	V00
212571	π Aqr	66 00	−44 44	4.79	0.23	B1 Ve	340	V00
217675	o And	102 12	−16 06	3.62	0.05	B6 IIIp	212	K94
219688	ψ² Aqr	67 37	−61 32	4.40	0.01	B5 V	99	V03

Table 3. SMC sight lines.

Star	AzV	RA (J2000) DEC ($^{h\,m\,s}$)	($^{\circ\,\prime\,\prime\prime}$)	V	$B-V$	$E(B-V)$ tot/SMC	Type	Ref	v_{rad} (km s^{-1})	Runs
Sk 13	18	00 47 12.2	−73 06 33	12.44	0.03	0.20/0.16	B2 Ia	1	138/147	V03
Sk 18	26	00 47 50.0	−73 08 21	12.46	−0.17	0.15/0.11	O7 III	1	142/149	V03
	47	00 48 51.5	−73 25 59	13.44	−0.18	0.13/0.09	O8 III	2	128/135	V02
Sk 40	78	00 50 38.4	−73 28 18	11.05	−0.05	0.14/0.10	B1 Ia+	3	164/155:	V03
	80	00 50 43.8	−72 47 42	13.32	−0.13	0.19/0.15	O4-6n(f)p	2	131/133	V04
	95	00 51 21.6	−72 44 15	13.78	−0.18	0.14/0.10	O7 III	2	137/136	V04
	120	00 52 20.4	−72 09 10	14.43	−0.22	0.09/0.05	O9 V	4	.../197	V04
	207	00 58 33.2	−71 55 47	14.25	−0.20	0.12/0.08	O7 V	4	.../141	V02
	321	01 02 57.1	−72 08 09	13.76	−0.19	0.12/0.08	O9 IInp	5	.../ 95	V04
	388	01 05 39.5	−72 29 27	14.09	−0.21	0.11/0.07	O4 V	4	.../168	V02
	440	01 08 56.0	−71 52 47	14.48	−0.18	0.13/0.09	O8 V	6	.../191	V04
Sk 143	456	01 10 55.8	−72 42 56	12.83	0.10	0.36/0.32	O9.7 Ib	7	169/...	E01
	476	01 13 42.5	−73 17 30	13.52	−0.09	0.23/0.19	O6.5 V	4	.../...	V03
Sk 155	479	01 14 50.3	−73 20 18	12.46	−0.15	0.13/0.09	O9 Ib	8	173/158	V03
Sk 190		01 31 28.0	−73 22 14	13.54	−0.18	0.11/0.07	O8 Iaf	4	.../176	V04

Photometry is from Massey (2002) (preferred) or from Dachs (1970), Azzopardi, Vigneau & Macquet (1975), Ardeberg & Maurice (1977), Bouchet et al. (1985), and/or Gordon et al. (2003). $E(B-V)$ is calculated using the intrinsic colours of FitzGerald (1970), assuming a Galactic contribution of 0.04 mag. Spectral types are from 1 = Garmany, Conti & Massey (1987); 2 = Walborn et al. (2000); 3 = Trundle & Lennon (2005); 4 = Massey (2002); 5 = Walborn et al. (2010); 6 = Massey et al. (2005); 7 = Fitzpatrick (1985a); 8 = Lennon 1997. Radial velocities are from Maurice, Bouchet & Martin (1989), Evans et al. (2004) and/or Welty & Crowther (in preparation); values with a colon are less well determined.

Table 4. LMC sight lines.

Star	HD	RA (J2000) DEC ($^{h\,m\,s}$)	($^{\circ\,\prime\,\prime\prime}$)	V	$B-V$	$E(B-V)$ tot/LMC	Type	Ref	v_{rad} (km s^{-1})	Runs
Sk−67 2	270754	04 47 04.5	−67 06 53	11.26	0.07	0.26/0.24	B1 Ia+	1	309/...	V03
Sk−67 5	268605	04 50 18.9	−67 39 38	11.34	−0.12	0.14/0.11	O9.7 Ib	2	309/...	V03
Sk−66 18		04 55 59.8	−65 58 30	13.50	−0.20	0.12/0.10	O6 V((f))	3	.../292	V04
LH 10-3061		04 56 42.5	−66 25 18	13.68	−0.01	0.31/0.28	O2 III	4	.../311	V04
Sk−69 50		04 57 15.1	−69 20 20	13.31	−0.16	0.12/0.03	O7(n)(f)p	5	.../214	V04
Sk−67 22		04 57 27.4	−67 39 03	13.44	−0.18	0.12/0.07	O2If/WN5	6	.../388	V04
Sk−67 38		05 03 29.7	−67 52 25	13.66	−0.22	0.09/0.04	O8 III	7	286/299	V04
Sk−70 69		05 05 18.7	−70 25 50	13.95	−0.23	0.09/0.01	O5 V	8	.../262	V02
Sk−68 41		05 05 27.1	−68 10 03	12.01	−0.14	0.08/0.02	B0.5 Ia	9	239/237	V02
Sk−68 52	269050	05 07 20.4	−68 32 09	11.63	−0.07	0.18/0.12	B0 Ia	10	234/218:	V03
BI 128		05 18 19.8	−65 49 15	13.82	−0.25	0.06/0.01	O9 V	3	.../313	V04
Sk−65 47		05 20 54.7	−65 27 18	12.60	−0.16	0.15/0.10	O4 I(n)f+p	5	.../227	V04
Sk−68 73	269445	05 22 59.8	−68 01 47	11.45	0.27	0.40/0.34	Of/WN	11	.../...	V03
Sk−67 101		05 25 56.3	−67 30 29	12.67	−0.23	0.08/0.03	O8 II	2	.../294	V02
BI 170		05 26 47.7	−69 06 12	13.06	−0.20	0.07/0.01	O9.5 Ib	2	.../265	V02
Sk−66 100		05 27 45.5	−66 55 15	13.26	−0.21	0.11/0.06	O6 II	8	309/304	V04
Sk−67 169		05 31 51.6	−67 02 22	12.18	−0.12	0.07/0.02	B1 Ia	9	.../289	V02
Sk−67 168	269702	05 31 52.1	−67 34 20	12.09	−0.17	0.12/0.07	O8 Iaf	9	.../242	V04
Sk−67 211	269810	05 35 13.9	−67 33 28	12.29	−0.21	0.10/0.04	O2 III	4	264/270	V02
BI 229		05 35 32.2	−66 02 38	12.95	−0.17	0.15/0.10	O7 V-III	2	.../305	V02
BI 237		05 36 14.6	−67 39 19	13.89	−0.12	0.20/0.14	O2 V	12	.../378	V04
Sk−66 171		05 37 02.4	−66 38 37	12.21	−0.15	0.13/0.08	O9 Ia	9	.../400	V04
BI 253		05 37 34.5	−69 01 10	13.76	−0.09	0.23/0.17	O2 V	4	.../271	V04
Sk−68 135	269896	05 37 49.1	−68 55 02	11.36	0.00	0.26/0.20	ON9.7 Ia+	10	290/291	V03
Melnick 42		05 38 42.2	−69 05 54	12.71	0.00	0.30/0.24	O2If/WN5	6	.../254	V02
Sk−69 246	38282	05 38 53.4	−69 02 01	11.10	−0.12	0.18/0.12	WN6h	13	.../...	V03
BI 272		05 44 23.1	−67 14 29	13.27	−0.19	0.13/0.07	O7 III-II	2	.../365:	V02
Sk−70 115	270145	05 48 49.7	−70 03 58	12.24	−0.10	0.20/0.14	O6.5 Iaf	14	.../278:	V02,V03

Photometry is from Massey (2002) or Parker 1993 (preferred) or from Ardeberg et al. (1972), Brunet et al. (1975), Isserstedt (1975, 1979, 1982), Feitzinger & Isserstedt (1983); and/or Schmidt-Kaler et al. (1999). $E(B-V)$ is calculated using the intrinsic colours of FitzGerald (1970); Galactic foreground extinction is estimated from fig. 13 of Staveley-Smith et al. (2003). Spectral types are from 1 = Fitzpatrick (1991), 2 = Walborn et al. (2002b), 3 = Massey et al. (1995), 4 = Walborn et al. (2002c), 5 = Walborn et al. (2010), 6 = Crowther (priv. comm.), 7 = Massey (2002), 8 = Walborn et al. (1995), 9 = Fitzpatrick (1988), 10 = Walborn (1977), 11 = Crowther & Smith (1997), 12 = Massey et al. (2005), 13 = Crowther & Dessart (1998), 14 = Walborn et al. (in preparation). Radial velocities are from Ardeberg et al. (1972), Fehrenbach & Duflot (1982), Walborn et al. (2002b) and/or Welty & Crowther (in preparation).

Th–Ar lamp spectra used for wavelength calibration. Because no near-UV filter was available for the auto-guider and because the targets could not always be observed close to the meridian, slight offsets generally were required to position the slit on the centroid of the stellar flux near the Ti II λ3383 line. Multiple exposures, of lengths typically 30–60 min, were obtained for most of the targets, with small night-to-night shifts of the spectral format on the detector to reduce the effects of any instrumental artefacts. Standard routines within IRAF were used to remove bias and to divide sections of the 2D spectral images containing the order(s) of interest by a normalized flat-field derived from quartz lamp exposures. The 1D spectra then were extracted from the flat-fielded image segments via the APEXTRACT routines, using variance weighting. Wavelength calibration was accomplished via Th–Ar lamp exposures, which were obtained several times during the course of each night, using the thorium rest wavelengths tabulated by Palmer & Engelman (1983). Multiple spectra for a given target were sinc interpolated to a common heliocentric wavelength grid, then summed. The summed spectra were then normalized via Legendre polynomial fits to the continuum regions surrounding the interstellar (and stellar) absorption lines. A signal-to-noise (S/N) ratio of about 220 (per half resolution element) was achieved near the λ3383 line in a total exposure time of 480 min for ζ Oph ($U = 1.7$); the corresponding 3σ equivalent width limit (assuming equal contributions from photon noise and continuum placement uncertainties) for a single component with line width $b = 2\,\mathrm{km\,s^{-1}}$ would be about 0.5 mÅ. Equivalent widths measured from these high-resolution spectra generally agree well with published values derived from lower resolution spectra (Table A2). Detailed comparisons with the corresponding high-resolution Ca II profiles (e.g. Welty et al. 1996) indicate that the differences in velocity zero point are $\lesssim 0.5\,\mathrm{km\,s^{-1}}$ in most cases.

Somewhat lower resolution spectra of nine (mostly) fainter, more reddened Galactic stars ($5.0 \lesssim V \lesssim 6.4$) were obtained with the coudé feed telescope in 2000 (run K00), using camera 5, grism 780-2, the 3° wedge and the BG3+CuSO$_4$ filters. The wider slit used with the camera 5 set-up, corresponding to 1.8 arcsec on the sky, yielded a resolution of about $3.4\,\mathrm{km\,s^{-1}}$ over the wavelength range from about 3240 to 3815 Å. The S/N ratios in the summed spectra range from about 40 to 80, with corresponding 3σ equivalent width limits of 2–4 mÅ, for these fainter targets. The λ3383 equivalent widths measured for o Per and 23 Ori agree well with previous values; the equivalent width for ζ Per (based on a single exposure) lies at the low end of the range of published values (Table A2).

2.2.2 ESO VLT + UVES

Spectra of seven Galactic, five SMC and seven LMC stars were obtained in 2003 November using the ESO/VLT UT2 telescope and UVES spectrograph (run V03; Dekker et al. 2000), under programme 72.C-0682, which was aimed at detecting weak interstellar atomic and molecular absorption lines towards stars in the Magellanic Clouds with relatively high column densities of Na I and/or H$_2$ (Welty et al. 2006). The standard dichroic 1 390/564 setting and a slit width corresponding to 0.7 arcsec were used to obtain nearly complete coverage of the wavelength range 3260–6680 Å – including lines from a number of interstellar atomic and molecular species. The spectral resolution, determined from the widths of the thorium lines in the Th–Ar lamp exposures used for wavelength calibration, was about $4.5\,\mathrm{km\,s^{-1}}$ near the Ti II λ3383 line. Multiple exposures, generally of length 20–45 min, were obtained for most of the Magellanic Clouds targets over the three nights, with the

camera tilted by ±50 units on the second and third nights to ensure that the spectra fell on slightly different parts of the CCD. The spectra were processed using standard routines within IRAF (as for the KPNO spectra), which produced extracted spectra essentially identical to those obtained with the UVES pipeline software for the observations obtained with the standard camera tilt. The S/N in the final summed spectra were typically ∼150–215 near the Ti II λ3383 line; corresponding 3σ detection limits for weak, unresolved absorption lines are ∼1.0–1.5 mÅ. Equivalent widths measured for the Ti II lines towards the Galactic stars ψ^2 Aqr and 23 Ori show very good agreement with previously reported values (Albert et al. 1993; Welty et al. 1999b; Table A2).

UVES spectra of the SMC star Sk 143, obtained using a very similar instrumental set-up in 2001 under programme 67.C-0281 (run V01; P. Ehrenfreund, PI), were retrieved from the European Southern Observatory (ESO) archive and processed with our IRAF-based procedure. This moderately reddened sight line has the highest known molecular fraction (Cartledge et al. 2005) and sole detection of CN absorption (Welty et al. 2006) in the SMC, and is the only SMC sight line known to exhibit a Milky Way-like extinction curve (with the 2175 Å extinction bump; Gordon et al. 2003). With one exception (see below), the equivalent widths and column densities (for various atomic and molecular species) derived from these spectra are consistent with those reported by Cox et al. (2007).

Spectra of nine SMC and 22 LMC stars were obtained in 2002 and 2004 (runs V02 and V04), under programmes 70.D-0164 and 74.D-0109, which were designed to investigate the atmospheric and wind properties of the target stars (e.g. Crowther et al. 2002; Evans et al. 2004). Most of these sight lines thus have somewhat lower hydrogen column densities and $E(B - V)$ than those probed in runs V01 and V03. The UVES pipeline reduction system (Ballester et al. 2000) was used to obtain the wavelength-calibrated extracted spectra used for analysis of the interstellar absorption lines. Because these observations employed a wider slit and generally shorter total exposure times, both the spectral resolution and S/N ratios (25–75) are somewhat poorer than those achieved in runs V01 and V03. Comparisons with higher resolution spectra, for several sight lines observed in runs V02 and V04, suggest that the actual achieved resolution is somewhat better than the nominal $8.7\,\mathrm{km\,s^{-1}}$ value cited in Table 1, however.

Spectra of 29 Galactic stars were obtained in 2000 under programme 65.I-0526 (run V00; E. Roueff, PI), which was aimed at detecting the weak molecular absorption lines of OH and NH towards reddened stars in the disc. All but three of the sight lines have $E(B - V) > 0.2$ mag, and six have $E(B - V) > 1.0$ mag. The raw spectral images were retrieved from the ESO archive and processed with the UVES pipeline reduction package (by A. Ritchey). The use of a very narrow slit yielded a resolution of about $3.8\,\mathrm{km\,s^{-1}}$ between about 3060 and 3860 Å; the S/N ratios range from about 225 to 455 (with 3σ equivalent width limits of 0.4–0.8 mÅ) near the λ3383 line. Several weaker Ti II lines near 3066, 3072, 3229 and 3241 Å are also included in these spectra. The equivalent widths measured for the Ti II λ3383 line and the Na I λ3302 lines are in good agreement with those reported by Hunter et al. (2006) for several sight lines in common.

The absorption features measured from the UVES spectra of the Magellanic Clouds targets from runs V01, V02, V03 and V04 for CH, CH$^+$ CN and several of the diffuse interstellar bands were discussed by Welty et al. (2006); the corresponding absorption lines from Na I, K I, Ca I, Ca II and Fe I will be described by Welty & Crowther (in preparation). The molecular absorption features found in the spectra of the Galactic targets from runs V00 and V03 are

included in a forthcoming survey of OH and NH absorption in translucent sight lines (Welty et al., in preparation).

2.2.3 HST (GHRS and STIS)

In order to perform detailed comparisons between the absorption-line profiles of Ti II and Zn II (typically at most very mildly depleted), high-resolution UV spectra including the Zn II lines at 2026 and/or 2062 Å were obtained for four Galactic, one SMC and two LMC sight lines. The four Galactic sight lines were originally observed under programmes 1360, 3415 (D. Ebbets, PI), and 3472 (L. Hobbs, PI) with the *Hubble Space Telescope* Goddard High Resolution Spectrograph, at resolutions of 3.4–3.7 km s^{-1}; the spectral data were reduced as described by Welty et al. (1999b). The three Magellanic Clouds sight lines were observed under GO programmes 8145 and 9757 (D. Welty, PI) with the *HST* Space Telescope Imaging Spectrograph, at a resolution of about 2.7 km s^{-1} (Welty et al. 2001, 2004, in preparation). Velocity alignment of the Zn II profiles was accomplished via fits to the adjacent lines of Mg I (λ2026) and Cr II (λ2062), using component structures derived from high-resolution optical spectra of similarly distributed Na I and Ca II, respectively (e.g. Welty et al. 1999b).

2.3 Spectra and equivalent widths

The normalized Galactic Ti II λ3383 line profiles are displayed, together with the corresponding Ca II λ3933 and K I λ7698 or Na I (λ5895, λ5889 or λ3302) profiles, in Appendix Fig. A1 (with online version of paper – see Supporting Information). The Ti II, Ca II and Na I profiles for the SMC and LMC sight lines (including absorption from both Galactic and Magellanic Clouds components) are shown in Appendix Fig. A2. The source of each spectrum is noted at the right, just above the continuum. For the Galactic sight lines, the zero point for LSR velocities is indicated by a solid triangle near the bottom of the frame. For the SMC and LMC targets, stellar radial velocities are indicated by asterisks (literature values) and/or the letter 'S' (values determined from our data); stellar absorption lines estimated in fits to the profiles are shown by dotted lines for some of the Ca II profiles. Individual interstellar components found in fits to the higher resolution Galactic line profiles are indicated by tick marks above the spectra; solid dots above the Na I or K I spectra show the velocities of components detected in CN absorption (an indicator of relatively dense gas). Note the differences in velocity scale for the various Galactic sight lines; the vertical dotted lines are separated by 10 km s^{-1} in all cases. Note also the expanded vertical scale for the weaker Galactic absorption lines; all lines towards the Magellanic Clouds targets are shown at the same (unexpanded) vertical scale, however. For a number of the LMC sight lines, the LMC Na I λ5889 (D2) absorption, at about -303 km s^{-1} relative to the λ5895 (D1) absorption, is blended with the Galactic D1 absorption near $v \sim 0$ km s^{-1}.

As seen in previous surveys (e.g. Stokes 1978; Hunter et al. 2006), the Ti II profiles often are very similar to those of Ca II, but can be very different from those of Na I and K I. In many sight lines (particularly in the LMC and SMC), the Ti II and Ca II absorption is spread over a wider range in velocity. In many of the Magellanic Clouds sight lines, the absorption from Ti II (and Ca II) is significantly stronger, relative to the absorption from Na I, than in most of the Galactic sight lines. Even the highest resolution Ti II profiles appear smoother, with less distinct component structure and very little absorption in very narrow components, compared to the

corresponding high-resolution Na I and K I profiles. As discussed below, such differences among the line profiles of those atomic species presumably reflect differences in the ionization and depletion behaviour (and thus distribution) of those species – and seem consistent with the Ti II primarily tracing warmer, more diffuse gas.

The equivalent widths $W(3383)$ for the Ti II λ3383 lines measured from the normalized spectra are listed in Table 5 (Milky Way sight lines) and Table 6 (MC sight lines); corresponding values for the weaker λ3072 and λ3241 lines are included for some of the Galactic sight lines observed in run V00. For the SMC and LMC sight lines, the absorption is separated into contributions from gas in our Galaxy (MW) and from gas in the Magellanic Clouds. Towards the SMC, the division is made at a (heliocentric) velocity of 60 km s^{-1}; towards the LMC, the division is made at $v = 100$ km s^{-1} (e.g. Lehner, Staveley-Smith & Howk 2009). For the Ti II absorption towards the LMC, separate values are listed for 'intermediate-velocity' absorption (100 km s$^{-1} \lesssim v \lesssim 200$ km s^{-1}) and for the 'main LMC' absorption ($v \gtrsim 200$ km s^{-1}). The 1σ uncertainties on the equivalent widths include contributions from both photon noise (Jenkins et al. 1973) and continuum placement (Sembach & Savage 1992); the latter generally dominates the total uncertainty for very broad absorption features.

Comparisons of $W(3072)$ versus $W(3383)$ and $W(3241)$ versus $W(3383)$ reveal essentially linear relationships, with slopes 0.31 ± 0.02 and 0.60 ± 0.02, respectively – very close to the values 0.28 and 0.59 expected from the ratios of $f\lambda^2$ for the three Ti II lines [using the rest wavelengths and oscillator strengths listed by Morton (2003)]. Those observed relationships thus suggest that the relative f-values are accurate and that saturation effects generally are not very significant, even for the strongest λ3383 line.

2.4 Column densities

Total sight line column densities were obtained from the normalized Ti II spectra both by integrating the apparent (instrumentally smeared) optical depth (AOD) over the line profile (Hobbs 1974; Savage & Sembach 1991) and by performing multicomponent fits to the line profiles (e.g. Welty et al. 2003). The AOD method can be used to obtain the apparent column density $N_a(v)$ as a function of velocity, but does not otherwise distinguish individual components in the profiles. Effects of saturation in the profiles may be estimated if several lines of different strength can be measured (Jenkins 1996). Fits to absorption-line profiles can yield column densities (N), line widths ($b \sim$ FWHM/1.665) and velocities (v) for individual components discernible in the spectra (given the resolution and S/N ratios characterizing the spectra and assuming that each component may be represented by a Voigt profile). While saturation effects are treated explicitly in the fits, having several lines of different strength can provide important constraints on N and b.

Fits to high-resolution spectra of Na I, K I and Ca II, for Galactic sight line samples having significant overlap with the present Ti II sample, have suggested that most of the sight lines contain multiple, closely blended components, with median separation of order 1.2–1.3 km s^{-1} (Welty et al. 1994, 1996; Welty & Hobbs 2001). The median component b-values for those samples are $\sim$0.7 km s^{-1} for Na I and K I and $\sim$1.3 km s^{-1} for Ca II; the larger value for Ca II reflects a population of broader components (likely representing warmer, more diffuse gas) not detected in the other two species. Similar complex structure is seen in the high-resolution Na I spectra available for a small number of Magellanic Clouds targets (Pettini & Gillingham 1988; Welty et al. 1999a; Welty & Crowther, in preparation).

Table 5. Galactic Ti ɪɪ equivalent widths.

HD	Name	Run	S/N	$W_\lambda(3072)$	$W_\lambda(3241)$	$W_\lambda(3383)$
23180	o Per	K00	80	–	–	5.9 ± 1.1
24398	ζ Per	K00	75	–	–	2.8 ± 0.8
24534	X Per	K00	60	2.9 ± 1.0	–	7.8 ± 1.6
24760	ϵ Per	K94	210	–	–	5.7 ± 0.5
27778	62 Tau	K00	40	–	–	5.0 ± 2.0
32630	η Aur	K95	95	–	–	1.9 ± 0.7
35149	23 Ori	K00	75	–	–	6.6 ± 1.3
		V03	125	–	–	5.8 ± 1.0
36486	δ Ori	K95	215	–	–	3.9 ± 0.8
37022	θ^1 Ori C	K00	55	–	–	10.2 ± 2.4
37043	ι Ori	K95	215	–	–	8.0 ± 0.6
37128	ϵ Ori	K94	280	–	–	8.6 ± 0.8
37742	ζ Ori	K95	175	–	–	5.2 ± 0.9
47839	S Mon A	K45	115	–	–	22.1 ± 2.1
	Walker 67	V03	55	–	–	10.9 ± 2.5
62542		V03	85	–	–	12.6 ± 2.4
72127A		V03	130	–	–	17.0 ± 2.6
72127B		V03	105	–	–	17.2 ± 1.5
73882		V03	90	–	–	51.6 ± 3.2
91316	ρ Leo	K95	335	–	–	29.7 ± 0.7
106625	γ Crv	V00	435	–	–	1.4 ± 0.1
110432		V00	355	–	4.9 ± 0.4	10.4 ± 0.4
112244		V00	435	9.4 ± 1.0	17.5 ± 0.5	31.6 ± 0.5
113904	θ Mus	V00	265	19.1 ± 2.2	36.0 ± 1.2	66.7 ± 1.4
114213		V00	265	24.8 ± 3.9	69.0 ± 1.9	93.1 ± 1.2
116658	α Vir	K95	455	–	–	0.8 ± 0.2
141637	1 Sco	K95	35	–	–	$15. \pm 4.$
143018	π Sco	K95	245	–	–	4.0 ± 0.7
144217	β^1 Sco	K95	225	–	–	7.2 ± 0.7
147165	σ Sco	K95	190	–	–	13.0 ± 0.8
147701		V00	250	–	15.1 ± 1.1	19.2 ± 1.4
147888	ρ Oph D	V00	255	–	9.1 ± 0.8	13.0 ± 0.6
147889		V00	305	–	5.0 ± 0.6	9.5 ± 0.7
147933	ρ Oph A	V00	325	5.7 ± 1.3	9.1 ± 0.7	14.0 ± 0.6
148184	χ Oph	V00	285	3.9 ± 1.0	9.6 ± 0.7	13.1 ± 0.6
148379		V00	315	21.6 ± 1.8	–	69.8 ± 0.8
149404		V00	225	18.7 ± 1.8	29.4 ± 0.8	52.5 ± 1.0
149757	ζ Oph	K45	220	–	–	9.1 ± 0.8
		V00	455	2.5 ± 0.7	7.0 ± 0.4	9.5 ± 0.3
150136		V00	305	–	23.2 ± 0.6	38.1 ± 0.7
152236	ζ^1 Sco	V00	315	14.9 ± 1.4	–	56.9 ± 1.0
154368		V00	315	8.9 ± 1.5	20.3 ± 0.8	36.1 ± 0.8
159561	α Oph	K45	185	–	–	4.6 ± 0.4
161056		V00	270	4.9 ± 1.3	11.9 ± 0.7	20.9 ± 0.7
166734		V00	325	–	53.2 ± 0.7	87.0 ± 0.9
167971		V00	305	21.7 ± 2.1	42.5 ± 0.8	71.0 ± 0.9
	BD−14 5037	V00	370	33.4 ± 2.1	–	98.5 ± 0.6
169454		V00	255	34.2 ± 1.9	64.6 ± 1.2	105.2 ± 1.0
170740		V00	295	–	–	16.0 ± 0.5
172028		V00	280	–	15.6 ± 1.0	23.8 ± 0.7
182985		V00	415	–	1.7 ± 0.3	4.9 ± 0.4
183143		V00	305	–	44.5 ± 0.8	67.4 ± 0.9
188220		V00	325	–	4.3 ± 0.5	5.9 ± 0.4
197345	α Cyg	K94	155	–	–	15.4 ± 0.7
199579		K00	65	–	–	17.9 ± 2.1
205637	ϵ Cap	V00	455	–	6.1 ± 0.4	13.4 ± 0.4
206267		K00	65	–	–	40.2 ± 2.2
207198		K00	60	–	–	47.1 ± 2.9
210121		V00	370	7.7 ± 0.7	12.2 ± 0.5	26.7 ± 0.6
212571	π Aqr	V00	455	5.7 ± 0.5	9.7 ± 0.4	17.0 ± 0.3
217675	o And	K94	145	–	–	5.6 ± 0.5
219688	ψ^2 Aqr	V03	205	–	–	2.1 ± 0.6

Entries are equivalent width $\pm 1\sigma$ uncertainty (mÅ). S/N values are per half resolution element near 3383 Å. Run K45 refers to sum of spectra from runs K94 and K95. W(3072) for X Per is from archival *HST* spectra.

Table 6. Magellanic Clouds Ti II λ3383 equivalent widths.

Star	S/N	MW	IV	MC
Sk 13	165	22.8 ± 1.8	–	281.0 ± 4.2
Sk 18	190	20.3 ± 1.4	–	231.0 ± 2.2
AV 47	40	22.8 ± 4.4	–	185.9 ± 11.5
Sk 40	110	26.2 ± 2.3	–	233.0 ± 4.1
AV 80	47	17.6 ± 3.8	–	200.3 ± 12.5
AV 95	39	22.9 ± 5.2	–	209.1 ± 17.7
AV 120	32	26.3 ± 5.2	–	76.5 ± 10.1
AV 207	25	21.1 ± 6.1	–	100.8 ± 17.1
AV 321	42	16.5 ± 4.0	–	44.1 ± 3.1
AV 388	30	27.5 ± 6.9	–	46.8 ± 8.3
AV 440	26	24.4 ± 7.7	–	115.7 ± 22.2
Sk 143	60	28.1 ± 5.3	–	36.2 ± 8.1
AV 476	85	24.1 ± 2.7	–	202.0 ± 4.0
Sk 155	195	32.9 ± 1.8	–	121.2 ± 3.6
Sk 190	40	39.5 ± 10.0	–	48.0 ± 9.1
Sk−67 2	150	28.5 ± 1.4	–	45.6 ± 2.2
Sk−67 5	190	31.9 ± 1.5	–	61.2 ± 1.0
Sk−66 18	45	26.8 ± 4.2	–	53.6 ± 6.2
LH 10-3061	40	36.7 ± 5.4	–	109.9 ± 7.8
Sk−69 50	47	32.1 ± 3.8	11.8 ± 2.5	55.9 ± 5.6
Sk−67 22	53	40.8 ± 4.1	–	61.7 ± 9.3
Sk−67 38	44	36.5 ± 5.0	–	24.1 ± 11.6
Sk−70 69	43	44.3 ± 3.4	–	13.8 ± 4.8
Sk−68 41	32	35.5 ± 6.1	–	10.2 ± 4.3
Sk−68 52	190	33.1 ± 1.7	–	115.0 ± 2.4
BI 128	28	29.3 ± 5.0	–	38.9 ± 12.0
Sk−65 47	57	45.9 ± 8.3	–	32.2 ± 8.3
Sk−68 73	190	33.3 ± 1.2	4.0 ± 0.9	102.9 ± 1.5
Sk−67 101	55	29.0 ± 2.2	5.8 ± 3.3	58.2 ± 5.1
BI 170	45	37.9 ± 3.9	9.1 ± 3.2	90.9 ± 6.6
Sk−66 100	48	37.0 ± 3.2	–	45.4 ± 5.3
Sk−67 169	31	31.1 ± 3.9		17.9 ± 6.4
Sk−67 168	53	35.6 ± 7.4		30.0 ± 6.6
Sk−67 211	70	30.6 ± 2.1	–	76.1 ± 4.6
BI 229	48	36.6 ± 3.4	–	17.9 ± 4.4
BI 237	38	39.1 ± 9.9	–	97.6 ± 9.4
Sk−66 171	31	49.2 ± 14.3	–	35.7 ± 11.8
BI 253	42	57.6 ± 11.3	–	169.6 ± 7.0
Sk−68 135	215	34.9 ± 1.6	4.8 ± 0.9	159.1 ± 2.4
Mk 42	38	39.0 ± 4.4	–	154.7 ± 10.9
Sk−69 246	215	45.2 ± 2.4	1.1 ± 0.6	136.1 ± 1.8
BI 272	54	34.8 ± 3.1	–	59.9 ± 5.5
Sk−70 115	190	42.0 ± 2.3	–	182.6 ± 2.9
	75	36.6 ± 4.4	–	179.7 ± 7.6

Entries are equivalent width ±1σ uncertainty (mÅ). For SMC sight lines, MW is for $v \lesssim 60 \, \mathrm{km \, s^{-1}}$; MC is for $v \gtrsim 60 \, \mathrm{km \, s^{-1}}$. For LMC sight lines, MW is for $v \lesssim 100 \, \mathrm{km \, s^{-1}}$; IV is for $100 \, \mathrm{km \, s^{-1}} \lesssim v \lesssim 200 \, \mathrm{km \, s^{-1}}$; MC is for $v \gtrsim 200 \, \mathrm{km \, s^{-1}}$.

Because of the relative weakness and comparative smoothness of the Ti II absorption, it is generally difficult to discern such complex structure for Ti II, even in the highest resolution Ti II spectra. The observed similarities between the Ti II and Ca II profiles and the roughly constant $N(\mathrm{Ti\,II})/N(\mathrm{Ca\,II})$ ratio (for total sight line values), however, suggest that those two species might (on the whole) be similarly distributed. We therefore fitted the Ti II profiles using the component structures derived from fits to the corresponding Ca II profiles, but only for sight lines where high-resolution (FWHM $\lesssim 2 \, \mathrm{km \, s^{-1}}$) Ca II spectra were available (e.g. Welty et al. 1996; Crawford 1995; Pan et al. 2004). In those fits, the relative velocities and most of the b-values were fixed to the values found for Ca II; the

individual component Ti II column densities and an overall velocity offset were allowed to vary.

The adopted Galactic interstellar component parameters are listed in Appendix Table A1 (with online version of paper – see Supporting Information); the individual components are noted by tick marks above the higher resolution spectra in Fig. A1. For each line of sight, the first line in Table A1 gives the source of the spectrum and (in square braces) the approximate 3σ column density limit for a single component with $b = 2 \, \mathrm{km \, s^{-1}}$. Subsequent lines give the component number and the heliocentric velocity, b-value, column density (in units of $10^{10} \, \mathrm{cm^{-2}}$) and ratio $N(\mathrm{Ti\,II})/N(\mathrm{Ca\,II})$ for that component. Component b-values in square braces were either varied or fixed (but relatively well determined) in the Ca II fits; values in parentheses also were fixed, but are less well determined.

For our Galactic sight lines, the total sight line column densities obtained from both AOD integrations and profile fits are included in Appendix Table A2 (a compilation of Galactic Ti II λ3383 equivalent widths and column densities from the literature). In most cases, the total Ti II column densities obtained from detailed profile fits (ours or others') are not more than 20 per cent (0.08 dex) higher than the values obtained from the AOD integrations (or directly from the equivalent widths) – a further indication that the Ti II λ3383 absorption is seldom significantly saturated. The few cases of larger differences (HD 42933, HD 74575, HD 179406) appear to be due to the adoption of very small b-values in the fits (Welsh et al. 1997) – which then require larger column densities to produce the observed absorption.

The adopted total sight line Ti II column densities for all our Galactic, SMC and LMC sight lines are listed in Tables 7, 8 and 9, respectively, together with the corresponding column densities of H I, H2 and Ca II and the Ti depletions obtained from $N(\mathrm{Ti\,II})$ and $N(H_{\mathrm{tot}}) = N(\mathrm{H\,I}) + 2N(\mathrm{H_2})$. For several Galactic sight lines where the λ3383 line is relatively weak and/or our spectrum is of fairly low S/N ratio (e.g. ζ Per, δ Ori), the Ti II column density in Table 7 is based on data from all available references. Where we have data for other Ti II lines (Table 5), the adopted $N(\mathrm{Ti\,II})$ is a weighted average of the values derived from all the lines. Tables 8 and 9 also include Ca II and Ti II column densities for a few Magellanic Clouds sight lines from previous studies (Caulet & Newell 1996; Cox et al. 2006, 2007).[2] For the LMC sight lines, separate values are given for the intermediate-velocity ($100 \lesssim v \lesssim 200 \, \mathrm{lm \, s^{-1}}$) and main LMC ($v \gtrsim 200 \, \mathrm{km \, s^{-1}}$) absorption for both Ca II and Ti II; the two are combined in the various correlation plots discussed below.

Nearly all of the Galactic, SMC and LMC H I column densities were derived from fits to the (damped) H I Lyman α absorption-line profiles, with corrections for stellar Lyman α absorption (for spectral types later than about B1) based on comparisons between stellar models and the Stromgren $[c_1]$ photometric index (Diplas & Savage 1994; Jenkins 2009). For HD 27778 (B3 V) and HD 147888 (B5 V), the corrections for stellar H I are the mean values for the respective spectral types (Diplas & Savage 1994); the adopted $N(\mathrm{H\,I})$ are consistent with the relationships observed in the Galactic ISM between $N(H_{\mathrm{tot}})$ and $E(B - V)$ (Bohlin, Savage & Drake 1978) and between $N(\mathrm{H\,I})$ and the equivalent width of the diffuse interstellar band at 5780 Å (Herbig 1993; Welty et al. 2006). For Be stars [HD 148184 (B2 IVpe), HD 212571 (B1 Ve)], where $[c_1]$ appears to be systematically lower than the values for the corresponding 'normal'

---

[2] The Ca II values of Cox et al. (2007) have not been adjusted for possible saturation effects; continuum placement may account for the differences in apparent column density derived from the H and K lines for some sight lines.

Table 7. Galactic column densities and Ti depletions.

Star	H I	H₂	Ca II	Ref	Ti II	D(Ti)
HD 23180	20.82	20.60	12.09	1/1	11.22	−2.86
HD 24398	20.80	20.67	11.96	1/1	11.09	−3.02
HD 24534	20.73	20.92	12.41	1/1	11.34	−2.92
HD 24760	20.45	19.52	11.59	1/1	11.20	−2.26
HD 27778	20.95	20.79	11.97	2/1	11.15	−3.10
HD 32630	–	–	11.22	–/1	10.79	–
HD 35149	20.56	18.30	12.10	1/1	11.22	−2.26
HD 36486	20.17	14.74	11.72	1/1	11.12	−1.97
HD 37022	21.54	<17.55	12.10	1/1	11.46	−3.00
HD 37043	20.20	14.69	11.93	1/1	11.39	−1.73
HD 37128	20.48	16.28	12.04	1/1	11.41	−1.99
HD 37742	20.39	15.86	11.97	1/1	11.18	−2.13
HD 47839	20.31	15.54	12.33	1/1	11.79	−1.44
Walker 67	–	–	12.28	–/1	11.49	–
HD 62542	20.90	20.81	11.96	2/1	11.54	−2.70
HD 72127A	–	–	12.97	–/1	11.68	–
HD 72127B	–	–	13.06	–/1	11.78	–
HD 73882	21.11	21.11	12.66	3/1	12.19	−2.32
HD 91316	20.44	15.61	12.03	1/1	11.93	−1.43
HD106625	–	–	10.84	–/1	10.59	–
HD110432	20.85	20.64	11.96	4/2	11.43	−2.69
HD112244	21.08	20.14	–	1/–	11.94	−2.15
HD113904	21.15	19.83	–	1/–	12.27	−1.84
HD114213	–	–	–	–/–	12.48	–
HD116658	19.00	12.95	10.76	5/1	10.36	−1.56
HD141637	21.18	19.23	11.51	1/1	11.72	−2.39
HD143018	20.66	19.32	10.93	1/1	11.04	−2.58
HD144217	21.03	19.83	11.73	1/1	11.31	−2.69
HD147165	21.38	19.79	11.86	1/1	11.58	−2.74
HD147701	–	–	–	–/–	11.79	–
HD147888	21.60	20.47	12.22	2/1	11.61	−2.97
HD147889	–	–	–	–/–	11.40	–
HD147933	21.63	20.57	12.15	1/1	11.61	−3.01
HD148184	21.13	20.63	11.99	2/1	11.58	−2.68
HD148379	–	–	–	–/–	12.32	–
HD149404	21.40	20.79	12.81	1/1	12.19	−2.30
HD149757	20.69	20.64	11.79	1/1	11.43	−2.62
HD150136	–	–	–	–/–	12.05	–
HD152236	21.77	20.73	13.08	1/1	12.23	−2.53
HD154368	21.00	21.16	12.66	6/1	12.02	−2.49
HD159561	–	–	11.53	–/1	11.12	–
HD161056	21.20	–	–	1/–	11.77	−2.35
HD166734	–	–	–	–/–	12.43	–
HD167971	21.60	20.85	–	7/–	12.33	−2.32
BD−14 5037	–	–	–	–/–	12.50	–
HD169454	–	–	–	–/–	12.54	–
HD170740	21.04	20.86	12.20	1/1	11.66	−2.67
HD172028	–	–	–	–/–	11.85	–
HD182985	–	–	–	–/–	11.15	–
HD183143	–	–	–	–/–	12.32	–
HD188220	–	–	11.56	–/3	11.26	–
HD197345	–	–	12.29	–/1	11.68	–
HD199579	21.04	20.53	12.61	1/1	11.71	−2.46
HD205637	–	–	–	–/–	11.54	–
HD206267	21.30	20.86	>12.56	7/4	12.09	−2.37
HD207198	21.34	20.83	>12.64	1/4	12.16	−2.31

Table 7 – *continued*

Star	H I	H₂	Ca II	Ref	Ti II	D(Ti)
HD210121	20.63	20.75	12.49	8/1	11.83	−2.28
HD212571	20.50	–	12.10	2/1	11.69	−1.73
HD217675	–	19.67	11.73	–/1	11.23	–
HD219688	–	–	10.99	–/1	10.76	–

Entries are log$N$ (cm^{-2}); limits are 3 σ. References are for H I and/or Ca II. References for H I: 1 = Diplas & Savage (1994); 2 = this paper; 3 = Fitzpatrick & Massa (1990); 4 = Rachford et al. (2001); 5 = York & Rogerson (1976); 6 = Snow et al. (1996); 7 = Rachford et al. (2002); 8 = Welty & Fowler (1992). References for H₂: Savage et al. (1977); Rachford et al. (2002, 2009). References for Ca II: 1 = Welty et al. (1996) and in preparation; 2 = Crawford (1995); 3 = Penprase (1993); 4 = Pan et al. (2004). Depletions are relative to a solar Ti/H = −7.08 dex.

H I column densities for the SMC and LMC are based directly on Lyman α data from *IUE* (Fitzpatrick 1985a,b, 1986; Gordon et al. 2003) or *HST* (Welty, in preparation); the H₂ column densities are primarily from the *FUSE* surveys of Tumlinson et al. (2002) and Cartledge et al. (2005).

The Ti depletions are determined relative to the stellar reference abundances listed in Table 10. For the Galactic sight lines, Ti/H = −7.08 dex (the solar photospheric value); for the SMC, Ti/H = −7.72 dex (an average for A, F, G and K supergiants); for the LMC, Ti/H = −7.24 dex (an average for F, G and K supergiants).

3 RESULTS

3.1 Comparisons with previous work

Some of the sight lines included in this study have previous measures of the Ti II λ3383 absorption, generally derived from spectra obtained at lower spectral resolution and/or lower S/N ratios. [Apart from the observations of ζ Per by Hobbs (1979) and of κ Vel by Dunkin & Crawford (1999), all previously reported Ti II spectra were obtained with instrumental FWHM $\gtrsim$ 3 km s^{-1} – i.e. at resolutions at least a factor of 2 poorer than our KPNO coudé feed/camera 6 spectra (see Appendix Table A2).] Sixteen of our Galactic sight lines were also observed by Stokes (1978), five were observed by Magnani & Salzer (1989, 1991), four were examined by Hunter et al. (2006), and a few others appear in various other studies (Table A2). In most cases, our equivalent widths and column densities agree with the previous values within the mutual 1σ uncertainties; weighted and unweighted fits to a comparison of our λ3383 equivalent widths with those of Stokes (1978), for example, yield slopes consistent with unity and intercepts consistent with zero.

Examination of the larger set of Ti II data in Table A2, however, reveals significant differences in the measured equivalent widths and/or derived column densities for some sight lines (e.g. towards β Ori, μ Col, ζ Pup, γ² Vel, HD 72127AB, θ Car, 9 Sgr, κ Aql, HD 206267). In principle, some of those differences could be due to temporal variations in the Ti II absorption, as have been seen for the trace species Na I and/or Ca II in a number of sight lines (Crawford 2003; Lauroesch 2007). While temporal variations in the absorption from dominant ions like Ti II have seldom been observed (e.g. Danks et al. 2001; Welty 2007), they would not be unexpected in sight lines probing disturbed regions – e.g. for HD 72127AB, which lies behind the Vela supernova remnant (Hobbs et al. 1991; Cha & Sembach 2000; Welty, Simon & Hobbs 2008). There appear to be differences among the Ti II profiles towards μ Col reported by Hobbs (1984),

spectral types, the mean corrections for the 'normal' types were used. For HD 62542 (B5 V), N(H I) was estimated via N(H$_{tot}$) = 5.8 × 10^{21} $E(B − V)$ (Bohlin et al. 1978) and the observed N(H₂) (Rachford et al. 2002). For the high-latitude star HD 210121 (B3 V), N(H I) was estimated from 21-cm emission (Welty & Fowler 1992). Except for Sk−69 202 (SN 1987A; Welty et al. 1999a), the

Table 8. SMC column densities and Ti depletions.

Star	$E(B-V)_{MC}$	H I	Ref	H$_2$	Ref	Ca II	Ref	Ti II	D(Ti)	Ref
Sk 13	0.16	22.04	1	20.36	1	13.04	1	12.98	−1.36	1
	–	–		–		12.93	2	12.95	–	2
Sk 18	0.11	21.70	1	20.63	2	12.83	1	12.90	−1.15	1
AV 47	0.09	21.30	1	17.77	2	12.70	1	12.82	−0.76	1
Sk 33	0.07	–		–		13.11	2	13.24		2
Sk 40	0.10	21.54	2	–		12.65	1	12.92	−0.90	1
AV 80	0.15	21.81	1	20.15	3	12.82	1	12.81	−1.30	1
AV 95	0.10	21.49	1	19.40	2	12.71	1	12.82	−0.96	1
AV 120	0.05	–		–		12.69	1	12.35	–	1
AV 207	0.08	21.43	1	19.40	2	12.77	1	12.49	−1.23	1
AV 214	0.25	21.40	3	–		12.86	2	12.86	−0.82	2
Sk 78	0.03	21.02	1	15.66	2	12.68	3	12.38	−0.92	3
Sk 85	0.03	21.30	1	17.21	2	12.74	2	12.64	−0.94	2
AV 321	0.08	–		<14.56	2	12.46	1	12.10	–	1
AV 388	0.07	21.15	1	19.40	2	12.33	1	12.14	−1.31	1
AV 398	0.29	21.90	3	–		13.16	2	13.16	−1.02	2
AV 440	0.09	21.36	1	–		12.59	1	12.57	−1.07	1
Sk 143	0.32	20.95	1	20.93	1	12.36	1	12.01	−1.68	1
	–	–		–		12.43	2	12.39	–	2
AV 476	0.19	21.85	1	20.95	3	12.85	1	12.82	−1.41	1
Sk 155	0.09	21.40	1	19.15	3	12.69	1	12.57	−1.11	1
Sk 190	0.07	–		–		12.27	1	12.14	–	1
Sk 191	0.10	21.51	1	20.65	3	12.21	2	12.17	−1.73	2

Entries are log N (cm^{-2}); limits are 3σ. SMC absorption is for $v > 60\,\mathrm{km\,s^{-1}}$.
Depletions are relative to stellar Ti/H = −7.72.
References for H I: 1 = Welty (in preparation); 2 = Fitzpatrick (1985a); 3 = Gordon et al. (2003).
References for H$_2$: 1 = Cartledge et al. (2005); 2 = Tumlinson et al. (2002); 3 = Welty et al. (in preparation).
References for Ca II: 1 = Welty & Crowther (in preparation); 2 = Cox et al. (2007); 3 = Sembach, Danks & Savage (1993) (see Welty & Crowther, in preparation).
References for Ti II: 1 = this paper; 2 = Cox et al. (2007); 3 = Roth et al. (1995) (see Welty et al. 2001).

Welsh et al. (1997), and Lallement et al. (2008) – particularly in the strength of the broad absorption feature from about 10 to 35 km s^{-1}, relative to that of the narrower component near +40 km s^{-1}. As the Ti II absorption is generally relatively weak and often spread over a fairly wide velocity range, however, many of the differences in equivalent width might just be due to differences in locating and fitting the local continuum; blending with weak, broad stellar lines may add further difficulty in defining the appropriate continuum towards later-type targets (e.g. for β Ori; Hobbs 1984; Welsh et al. 1997).

Five of the Magellanic Clouds sight lines listed in Tables 8 and 9 were also observed and analyzed by Cox et al. (2006, 2007). For four of those five sight lines, the derived SMC or LMC Ti II column densities agree within about 10 per cent (0.04 dex). The lone discrepancy – the factor of 2.4 difference in the SMC N(Ti II) towards Sk 143 – is somewhat puzzling, as the raw spectral data used in the two studies are the same, and as there is much better agreement between the derived Galactic Ti II column densities. Comparison of our normalized Ti II profile (Fig. A2) with the AOD profile for the λ3383 line in Cox et al. (2007) suggests that differences in the adopted continuum at SMC velocities are likely responsible for the difference in derived N(Ti II) in this case.

Observations of the Ti II λ3072 line towards a few stars have been reported by Federman, Weber & Lambert (1996) and Felenbok & Roueff (1996), in papers focused on the nearby OH absorption features. For several of those sight lines, the equivalent widths of the OH lines at 3078 and 3081 Å are in good agreement with previously reported values. The additional narrow blue-ward components seen in the Ti II line by Felenbok & Roueff towards both ζ Per and HD

27778 are not present in the λ3383 profiles (Fig. A1), however; they may be instrumental artefacts. The Ti II column densities obtained from the λ3072 equivalent widths are somewhat larger than those obtained from independent observations of the stronger λ3383 line (Table A2).

3.2 Ti II versus Ca II

Titanium and calcium are two of the most severely depleted elements in diffuse Galactic disc clouds (e.g. Jenkins 1987). Several previous studies have noted that the column density ratio N(Ti II)/N(Ca II) appears to be roughly constant in the Galactic ISM, with a value of 0.3–0.4 for clouds in both the disc and low halo (Stokes 1978; Albert 1983; Welsh et al. 1997; Hunter et al. 2006). Fig. 1 shows the relationship between the column densities of Ti II and Ca II for sight lines in our Galaxy and in the Magellanic Clouds (including well-determined values from other references).[3] In this figure (and in subsequent such figures), sight lines in the SMC and LMC are denoted by red triangles and green circles, respectively, with filled symbols representing detections (of both species) and open symbols representing limits (for one or both species). Galactic sight lines in the Orion Trapezium and Sco-Oph regions, which exhibit somewhat different abundances for some species (e.g. Welty &

[3] Compilations of column densities for Galactic and Magellanic Clouds sight lines (with uncertainties and references) are maintained at http://www.astro.illinois.edu/~dwelty/coldens.html and coldens_mc.html, respectively.

Table 9. LMC column densities and Ti depletions.

Star	$E(B-V)_{MC}$	H I	Ref	H$_2$	Ref	Ca II IV/LMC	Ref	Ti II IV/LMC	D(Ti)	Ref
Sk−67 2	0.24	21.00	1	20.95	1	11.00/12.12	1	12.13	−2.07	1
	−	−		−		12.32	2	12.16	−	2
Sk−67 5	0.11	21.00	2	19.48	2	11.27/12.19	1	12.28	−1.50	1
	−	−		−		12.26	2	12.30	−	2
Sk−66 18	0.10	−		−		11.04/12.32	1	12.20	−	1
LH 10-3061	0.28	−		−		11.55/12.44	1	12.55	−	1
Sk−69 50	0.03	−		−		12.18/12.31	1	11.51/12.13	−	1
Sk−67 22	0.07	21.11	2	−		11.08/12.11	1	12.26	−1.61	1
Sk−67 38	0.04	−		−		11.07/11.86	1	11.84	−	1
Sk−70 69	0.01	<20.50	2	<14.41	2	11.44/11.96	1	11.59	> −1.67	1
Sk−68 41	0.02	<20.50	2	<14.15	2	10.86/12.02	1	11.46	> −1.80	1
Sk−68 52	0.12	21.40	2	19.47	2	11.11/12.58	1	12.54	−1.63	1
BI 128	0.01	−		−		11.20/11.98	1	12.05	−	1
Sk−65 47	0.10	<20.50	2	−		10.89/12.11	1	11.96	> −1.30	1
Sk−68 73	0.34	21.60	2	20.09	3	11.96/12.55	1	11.04/12.52	−1.86	1
Sk−67 101	0.03	<20.50	2	<14.11	2	11.97/12.05	1	11.20/12.20	> −1.02	1
BI 170	0.01	<20.90	2	<13.95	2	11.71/12.46	1	11.40/12.39	> −1.23	1
Sk−66 100	0.06	<20.50	2	<14.25	2	11.32/12.08	1	12.12	> −1.14	1
Sk−67 169	0.02	−		<13.95	2	11.06/12.10	1	11.71	−	1
Sk−67 168	0.07	<20.70	1	−		11.90/12.05	1	11.93	> −1.53	1
Sk−67 211	0.04	20.70	2	<13.95	2	11.62/12.20	1	12.35	−1.11	1
Sk−69 202	0.13	(21.4)	2	−		11.86/12.59	3	12.34	−1.82	3
BI 229	0.10	20.70	2	<14.08	2	11.38/11.87	1	11.69	−1.77	1
BI 237	0.14	21.62	2	20.05	3	11.72/12.44	1	12.49	−1.89	1
Sk−69 223	−	−		20.07	3	12.68	2	12.77	−	2
Sk−66 171	0.08	<20.70	2	−		10.80/12.12	1	12.02	> −1.44	1
BI 253	0.17	21.60	2	19.70	3	11.36/12.73	1	12.75	−1.61	1
Sk−68 135	0.20	21.60	2	19.86	2	11.89/12.72	1	11.12/12.70	−1.67	1
	−	−		−		12.68	2	12.73	−	2
Mk 42	0.24	21.79	2	−		11.55/12.81	1	12.69	−1.86	1
Sk−69 243	−	21.80	3	−		12.88	2	12.76	−1.80	2
Sk−69 246	0.12	21.40	2	19.71	2	11.59/12.63	1	10.48/12.64	−1.54	1
Sk−69 274	0.13	−		−		11.74/12.58	1	12.76	−	4
Sk−69 282	0.12	21.51	1	−		11.78/12.71	4	12.74	−1.53	4
Sk−69 290	0.12	−		−		11.85/13.09	4	12.82	−	4
BI 272	0.07	<21.00	2	<14.21	2	11.72/12.13	1	12.25	> −1.51	1
Sk−70 115	0.14	21.30	2	19.94	2	10.45/12.40	1	12.77	−1.33	1
	−	−		−		12.48	4	12.81	−	4
Sk−70 120	0.06	−		−		12.59	2	12.63	−	2

Entries are $\log N$ (cm^{-2}); limits are 3σ. LMC absorption is for $v > 200$ km s^{-1}; IV absorption towards LMC is for $100 < v < 200$ km s^{-1}.
Depletions are relative to stellar Ti/H = −7.24.
References for H I: 1 = Fitzpatrick (1985b, 1986); 2 = Welty (in preparation); 3 = Bluhm & de Boer (2001).
References for H$_2$: 1 = Cartledge et al. (2005); 2 = Tumlinson et al. (2002); 3 = Welty et al. (in preparation).
References for Ca II: 1 = Welty & Crowther (in preparation); 2 = Cox et al. (2006); 3 = Welty et al. (1999a); 4 = Caulet & Newell (1996).
References for Ti II: 1 = this paper; 2 = Cox et al. (2006); 3 = Welty et al. (1999a); 4 = Caulet & Newell (1996).

Hobbs 2001), are denoted by blue asterisks and blue open squares, respectively. The solid lines show the weighted and unweighted fits to the Galactic data (generally not including the Trapezium or Sco-Oph sight lines).[4] The points for the Galactic ISM define a roughly

[4] The Sco-Oph sight lines include 1 Sco, π Sco, δ Sco, β^1 Sco, ω^1 Sco, σ Sco, ν Sco, τ Sco, o Sco, 22 Sco, HD 147701, ρ Oph (A-D) and HD 147889 – but not ζ Oph, χ Oph, 67 Oph, ζ^1 Sco, HD 154090 or HD 154368. The Trapezium sight lines include θ^1 Ori B, θ^1 Ori C, θ^2 Ori A and HD 37061. The fits were performed with a slightly modified version of the subroutine REGRWT.F, obtained from the statistical software archive maintained at Penn State (http://www.astro.psu.edu/statcodes); see Welty & Hobbs (2001). The fits accounted for the uncertainties in both dependent and independent variables, but did not consider limits.

linear trend – with slope ∼0.7, relatively small scatter (rms deviation ∼0.2 dex; correlation coefficient $r = 0.865$), and a few outliers (e.g. HD 72127AB, with Ti II/Ca II $\lesssim 0.05$ and κ Vel). The mean Ti II/Ca II ratio for this particular set of Galactic sight lines is ∼0.3, consistent with the values found in previous studies – though the ratio is somewhat higher (on average) towards the Sco-Oph stars and does decrease with increasing column density and/or increasing $E(B-V)$. The Magellanic Clouds sight lines appear to exhibit a somewhat steeper relationship, with slope $\gtrsim 1$ and a higher mean Ti II/Ca II ratio ∼0.9 for both the SMC and LMC (see also Cox et al. 2006, 2007). Most of the Galactic sight lines, however, primarily probe gas in the disc; the Galactic absorption seen towards the Magellanic Clouds targets (due to both disc and halo gas in those directions) falls somewhat above the mean Galactic trend, at

Table 10. Ti reference abundances.

Ti/H	Objects	Reference
	Milky Way	
−7.08	solar photosphere	Lodders (2003)
	SMC	
−7.71	10 A supergiants	Venn (1999)
−7.64	3 F-G supergiants	Spite, Spite & Francois (1989)
−7.59	8 F-G supergiants	Russell & Bessell (1989)
−7.61	7 F-G supergiants	Luck & Lambert (1992)
−7.65	6 F-G supergiants	Luck et al. (1998)
−7.68	6 K supergiants	Hill (1997)
−7.91	6 G-K supergiants	Hill (1999)
−7.87	7 G-K supergiants	Gonzalez & Wallerstein (1999)
−7.72	adopted value	
	LMC	
−7.24	8 F-G supergiants	Russell & Bessell (1989)
−7.28	7 F-G supergiants	Luck & Lambert (1992)
−7.13	9 F-G supergiants	Hill, Andrievsky & Spite (1995)
−7.22	10 F-G supergiants	Luck et al. (1998)
−7.31	1 K star	Spite, Barbuy & Spite (1993)
−7.24	adopted value	
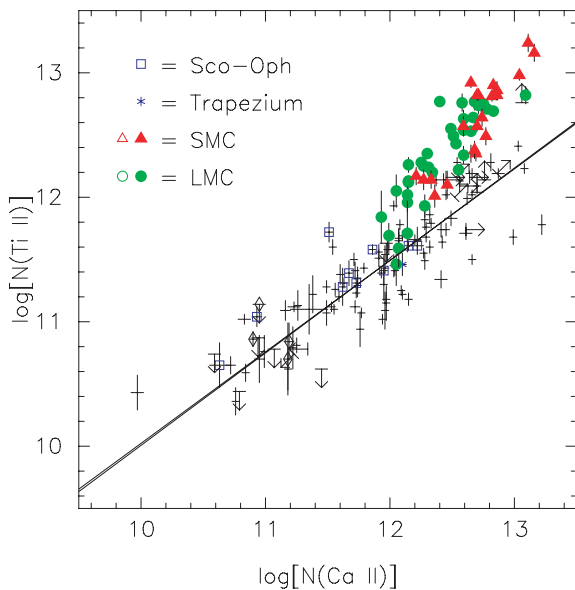
Figure 1. N(Ti II) vs. N(Ca II) for both Galactic and Magellanic Clouds sight lines. Green circles denote LMC sight lines and red triangles denote SMC sight lines (filled symbols for detections, open symbols for limits); blue open squares denote Sco-Oph sight lines; blue asterisks denote Orion Trapezium region sight lines; plus signs denote other Galactic sight lines (with size indicating $\pm 1\sigma$ uncertainties). The two (nearly indistinguishable) solid lines, with slopes ∼0.7, represent weighted and unweighted fits to the Galactic data (not including the Sco-Oph or Trapezium sight lines).

$(12.19 \pm 0.16, 11.89 \pm 0.13)$ towards the SMC and $(12.12 \pm 0.16, 12.05 \pm 0.10)$ towards the LMC.

As also noted previously (Stokes 1978; Albert et al. 1993), there are indications of a somewhat broader distribution of the Ti II/Ca II ratio for individual velocity components, compared to the range seen for integrated sight line values. The fits to the highest resolution

Galactic Ti II profiles (using the component structures determined from high-resolution spectra of Ca II) yield Ti II/Ca II ratios ranging from ∼0.05 to ∼5 (last column in Appendix Table A1). The lowest values are typically found for components with small b-values (often with corresponding strong, narrow Na I and/or K I lines) and/or for components also detected in CH and CN – which likely arise in relatively cold, dense gas. Even lower values, however, are found for some intermediate-velocity components towards HD 72127AB – where high Fe II/Zn II ratios suggest significant disruption of the dust grain populations (Welty et al. 2008). The highest Galactic Ti II/Ca II values in our sample are found for some of the higher velocity components ($-35\,\mathrm{km\,s^{-1}} \lesssim v \lesssim -20\,\mathrm{km\,s^{-1}}$) towards stars in the Sco-Oph region and for some components towards the low halo star ρ Leo.

Ratios of the apparent optical depths for Ti II and Ca II in the lower resolution UVES spectra of the Magellanic Clouds targets yield analogous information on the variation of Ti II/Ca II with velocity in each sight line. In both the SMC and LMC, the overall distributions of the Ti II/Ca II ratios peak at about 1.25; the individual ratios (for velocity intervals of 2–4 km s⁻¹) range from about 0.08 to 8.0.

3.3 Ti depletion

Previous surveys of Ti II absorption have explored the behaviour of the titanium depletions $D(\mathrm{Ti}) = \log[\delta(\mathrm{Ti})]$ in the disc and low halo of our Galaxy (e.g. Stokes 1978; Albert et al. 1993; Welsh et al. 1997; Hunter et al. 2006). Fig. 2 gives an updated version of the relationship between D(Ti) and the average sight line density $\langle n_{\mathrm{H}} \rangle = N(H_{\mathrm{tot}})/d$ (where d is the distance to the target star) for the Galactic sample (e.g. Albert et al. 1993). Figs 3–5 show the variations of D(Ti) with respect to the total hydrogen column density $N(H_{\mathrm{tot}})$, the colour excess $E(B - V)$ and the molecular fraction $f(H_2)$,
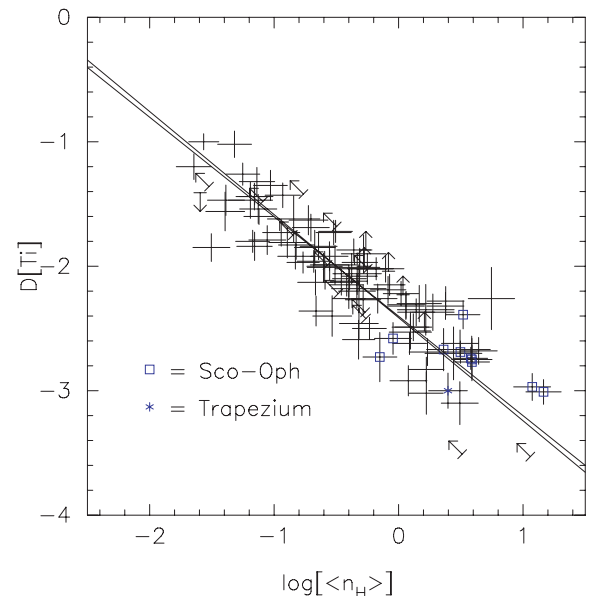
Figure 2. D(Ti) vs. mean sight line density $\langle n_{\mathrm{H}} \rangle$ for Galactic sight lines. Blue open squares denote Sco-Oph sight lines; blue asterisks denote Orion Trapezium region sight lines; plus signs denote other Galactic sight lines (with size indicating $\pm 1\sigma$ uncertainties). The depletions are relative to the solar Ti abundance. The two solid lines, with slopes ∼ −0.8, represent weighted and unweighted fits to the data (not including the Sco-Oph or Trapezium sight lines).
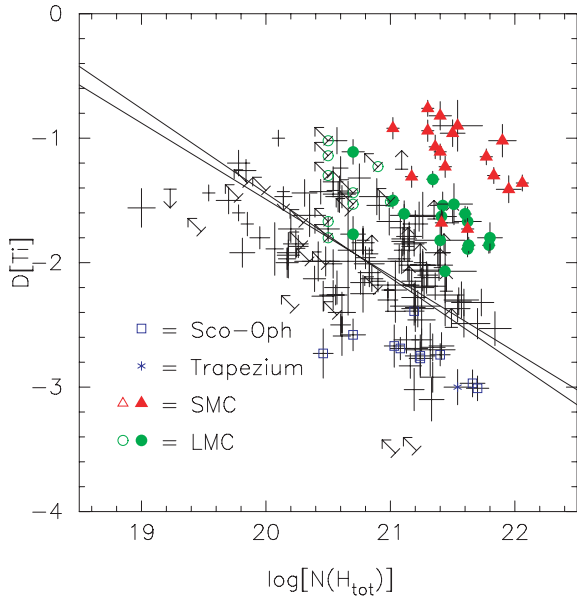
Figure 3. D(Ti) vs. $N(H_{tot})$ for both Galactic and Magellanic Clouds sight lines. Green circles denote LMC sight lines and red triangles denote SMC sight lines (filled symbols for detections, open symbols for limits); blue open squares denote Sco-Oph sight lines; blue asterisks denote Orion Trapezium region sight lines; plus signs denote other Galactic sight lines (with size indicating $\pm 1\sigma$ uncertainties). The depletions are relative to the solar Ti abundance for the Galactic sight lines and to the stellar Ti abundances for the SMC and LMC sight lines. The two solid lines, with slopes ~ -0.65, represent weighted and unweighted fits to the Galactic data (not including the Sco-Oph or Trapezium sight lines).

respectively, for the Milky Way, LMC and SMC. These figures are based on Ti II column density data (from this study and from other published studies) for 204 Galactic sight lines, 35 LMC sight lines and 21 SMC sight lines (though not all those sight lines have corresponding data for hydrogen). The titanium depletions in the Galactic sight lines range from about -1.0 dex (towards the distant, low halo star HD 93521) to about -3.1 dex (towards the relatively nearby, moderately reddened HD 27778) – very similar to the range seen in the less extensive compilation of Jenkins (2009). The depletions for the current sample of sight lines in the Magellanic Clouds (Tables 8 and 9) are generally less severe, ranging from -1.1 to -2.1 dex in the LMC and from -0.8 to -1.7 dex in the SMC – consistent with the Ti/H ratios found for smaller samples by Cox et al. (2006, 2007).[5] The most severe depletions in the Magellanic Clouds are found towards the moderately reddened stars Sk 143 (SMC) and Sk−67 2 (LMC) – the two sight lines with the highest molecular fractions and the only detections of CN absorption in the currently available sample (Cartledge et al. 2005; Welty et al. 2006).[6]

While the mean sight line density $\langle n_H \rangle$ is an imperfect indicator of the local hydrogen density, the relationship between D(Ti) and $\langle n_H \rangle$ is remarkably tight in the Galactic ISM, with slope ~ -0.8 and rms scatter ~ 0.17 dex – suggestive of more severe Ti depletion at higher n_H (though see Section 4.3). All three galaxies exhibit generally increasingly severe titanium depletions with increasing

$N(H_{tot})$ and $E(B - V)$, with similar slopes (~ -0.65) versus $N(H_{tot})$ and significant scatter (rms ~ 0.3 dex for the Galactic sight lines) at any given $N(H_{tot})$. On average, the titanium depletions towards the Trapezium and Sco-Oph targets are more severe than the average Galactic values at the corresponding $N(H_{tot})$, by a factor ~ 3 (though they appear more 'normal' versus $\langle n_H \rangle$); inclusion of those sight lines yields slopes ~ -0.7 versus $N(H_{tot})$, consistent with the value found by Wakker & Mathis (2000). A number of the Galactic sight lines with the least severe depletions [at a given $N(H_{tot})$] probe either relatively long paths through the lower Galactic halo (HD 93521, HD 149881, HD 215733) or somewhat disturbed regions (e.g. HD 93205 and HD 303308 in Carina). The depletions are typically even less severe in the Magellanic Clouds, by factors of ~ 5 in the LMC and ~ 20 in the SMC [at any given $N(H_{tot})$]. Although the differences among the three galaxies are smaller when viewed versus $E(B - V)$ (a consequence of the smaller dust-to-gas ratios in the Magellanic Clouds), the titanium depletions (on average) still are less severe in the LMC and SMC than in our sample of Galactic sight lines. While H_2 column densities are not known for some of the Magellanic Clouds sight lines in Fig. 3, examination of the available *FUSE* spectra indicates that $f(H_2)$ is generally less than about 0.1 in those cases (Welty et al., in preparation).

For molecular fractions less than 0.1, the Galactic titanium depletions appear to be roughly constant, with mean D(Ti) ~ -1.8 dex [and with considerable scatter at any given $f(H_2)$]. For $f(H_2) \gtrsim 0.1$, the mean D(Ti) is about -2.3 dex, and the depletions become increasingly severe with increasing $f(H_2)$; several sight lines with more than half the hydrogen in molecular form have D(Ti) $\lesssim -3.0$ dex. The Sco-Oph and Trapezium sight lines stand well apart from the general Galactic trend – reflecting a combination of fairly severe depletions [mean D(Ti) ~ -2.8 dex] and somewhat lower molecular fractions [versus other sight lines with comparable $N(H_{tot})$ or depletions]. While the depletions are again less severe for the LMC and SMC [at any given $f(H_2)$], the small sample size renders more quantitative estimates of the differences rather uncertain.

Because hydrogen column densities, colour excesses and molecular fractions cannot be determined directly for the individual components comprising the complex interstellar line profiles seen in most sight lines, it is more difficult to determine the depletion behaviour for individual interstellar clouds. For a small number of sight lines, however, high-resolution (FWHM ~ 2–$4\,km\,s^{-1}$) UV spectra of the absorption lines from relatively undepleted dominant ions (e.g. O I, Zn II, Kr I) may be used to estimate the total hydrogen column densities (and then the titanium depletions) in those individual components/clouds, via fits to the various absorption-line profiles. Alternatively, if the various absorption line profiles are placed on a common velocity grid, then ratios of the apparent optical depths [e.g. $\tau_a(Ti\,II)/\tau_a(Zn\,II)$] may be used to gauge the Ti depletion as a function of velocity.

Figs 6 and 7 compare high-resolution Ti II ($\lambda 3383$) and Zn II ($\lambda 2026$ or $\lambda 2062$) profiles for four Galactic and three Magellanic Clouds sight lines, respectively, sampling different regions/environments in each of the three galaxies: ϵ Ori is one of the belt stars in Orion, ρ Leo lies about 600 pc above the Galactic plane in the low halo, π Sco is one of the 'Sco-Oph' stars (exhibiting weak absorption from trace neutral and molecular species), ζ Oph shows relatively strong absorption from trace neutral and molecular species, Sk 155 is in the near 'wing' region of the SMC, Sk−67 5 is at the northwestern end of the main bar of the LMC, and Sk−70 115 lies within the LMC2 supershell (southeast of the 30 Doradus star-forming region). In each panel, the points in the top section

[5] The Ti depletions listed by Cox et al. (2007) for the SMC sight lines, however, are with respect to a Galactic reference abundance (-6.9 dex).

[6] While D(Ti) is listed as -1.73 dex for Sk 191 in Table 8, that sight line may be characterized by a somewhat lower metallicity than is typical for the SMC – in which case the depletion would be less severe.
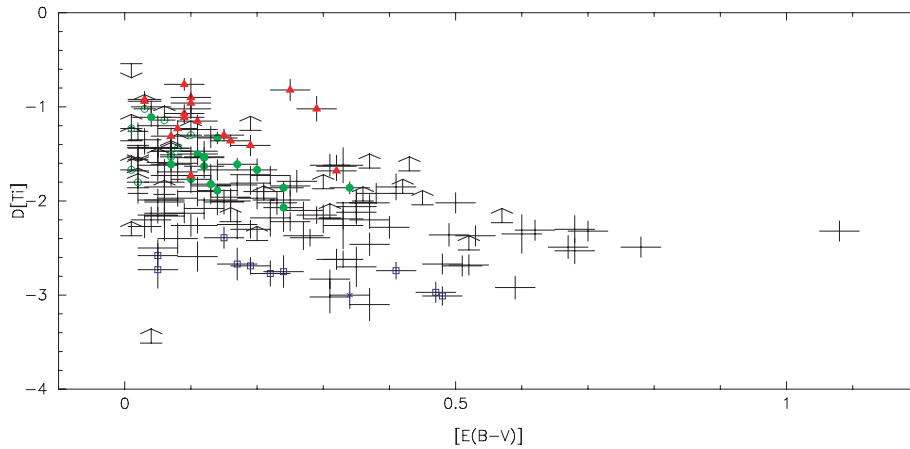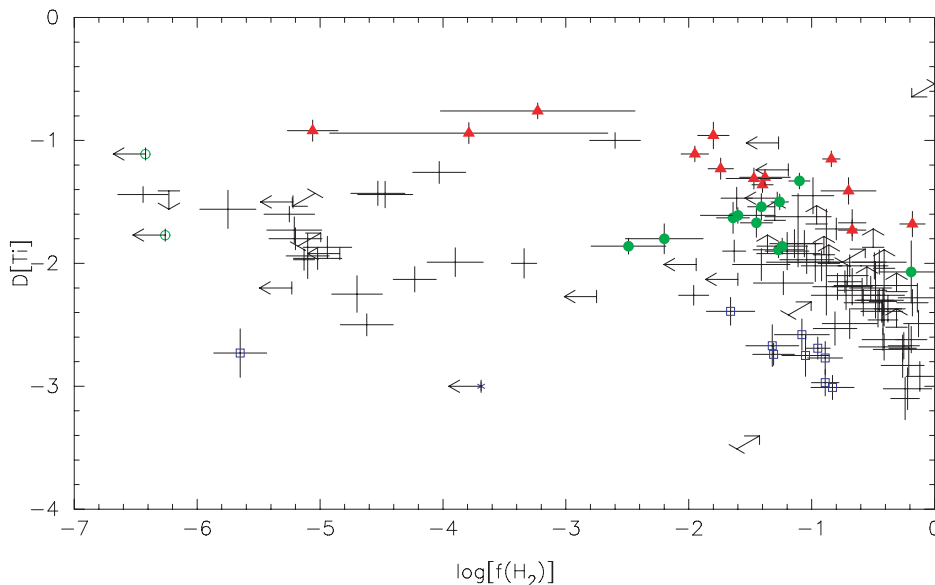
Figure 4. D(Ti) vs. $E(B - V)$ for both Galactic and Magellanic Clouds sight lines. Green circles denote LMC sight lines and red triangles denote SMC sight lines (filled symbols for detections, open symbols for limits); blue open squares denote Sco-Oph sight lines; blue asterisks denote Orion Trapezium region sight lines; plus signs denote other Galactic sight lines (with size indicating $\pm 1\sigma$ uncertainties). The depletions are relative to the solar Ti abundance in our Galaxy and to the stellar Ti abundances in the SMC and LMC.

Figure 5. D(Ti) vs. $f(H_2)$ for both Galactic and Magellanic Clouds sight lines. Green circles denote LMC sight lines and red triangles denote SMC sight lines (filled symbols for detections, open symbols for limits); blue open squares denote Sco-Oph sight lines; blue asterisks denote Orion Trapezium region sight lines; plus signs denote other Galactic sight lines (with size indicating $\pm 1\sigma$ uncertainties). The depletions are relative to the solar Ti abundance in our Galaxy and to the stellar Ti abundances in the SMC and LMC.

show the ratio [Ti/Zn], which should track any variations in the Ti depletion.[7] For the Galactic sight lines, the [Ti/Zn] ratios were determined from corresponding ratios of the apparent optical depths in the line profiles (after smoothing the Ti II spectra to the lower resolution of the Zn II spectra). For the Magellanic Clouds sight lines, the [Ti/Zn] ratios were determined from detailed, simultaneous, multicomponent fits to the profiles of lines from a number of dominant ions (Welty et al. 2001; Welty et al. 2004, and in preparation). The letters H, W and C (at the upper right in each panel) give representative values for [Ti/Zn] for clouds in the low Galactic

halo (-0.6 dex); warm, diffuse clouds in the disc (-1.35 dex); and colder, denser disc clouds (-2.55 dex) (Savage & Sembach 1996; Welty et al. 1999b; updated for more recent solar and interstellar abundance data; see also Jenkins 2009).

In general, the Ti II and Zn II absorption-line profiles span very similar velocity ranges, but the profiles may be quite different in detail. While the Ti II and Zn II profiles are broadly similar towards both ϵ Ori and ρ Leo, for example, there are still differences of nearly an order of magnitude in [Ti/Zn] for different velocity intervals. The profiles of the two species are very different towards π Sco and ζ Oph, however, with correspondingly larger ranges in [Ti/Zn] or D(Ti). Towards π Sco, [Ti/Zn] ranges from about -1.4 to < -3.2 dex (versus -2.4 dex for the sight line as a whole); towards ζ Oph, [Ti/Zn] ranges from about -1.3 to $\lesssim -2.7$ dex (the strongest Zn II components may be somewhat saturated). Estimates for $N(H_{\text{tot}})$ based on detailed fits to the Zn II profiles towards ζ Oph

---

[7] $[\text{Ti}/\text{Zn}] = \log[N(\text{Ti II})/N(\text{Zn II})] - \log(\text{Ti}/\text{Zn})_0$, where $(\text{Ti}/\text{Zn})_0$ is the solar (0.29 dex) or stellar reference ratio. Since the corresponding [Zn/H] ratios are typically $\gtrsim -0.4$ dex, [Ti/Zn] is generally a reasonably good indicator of the Ti depletion in predominantly neutral gas.
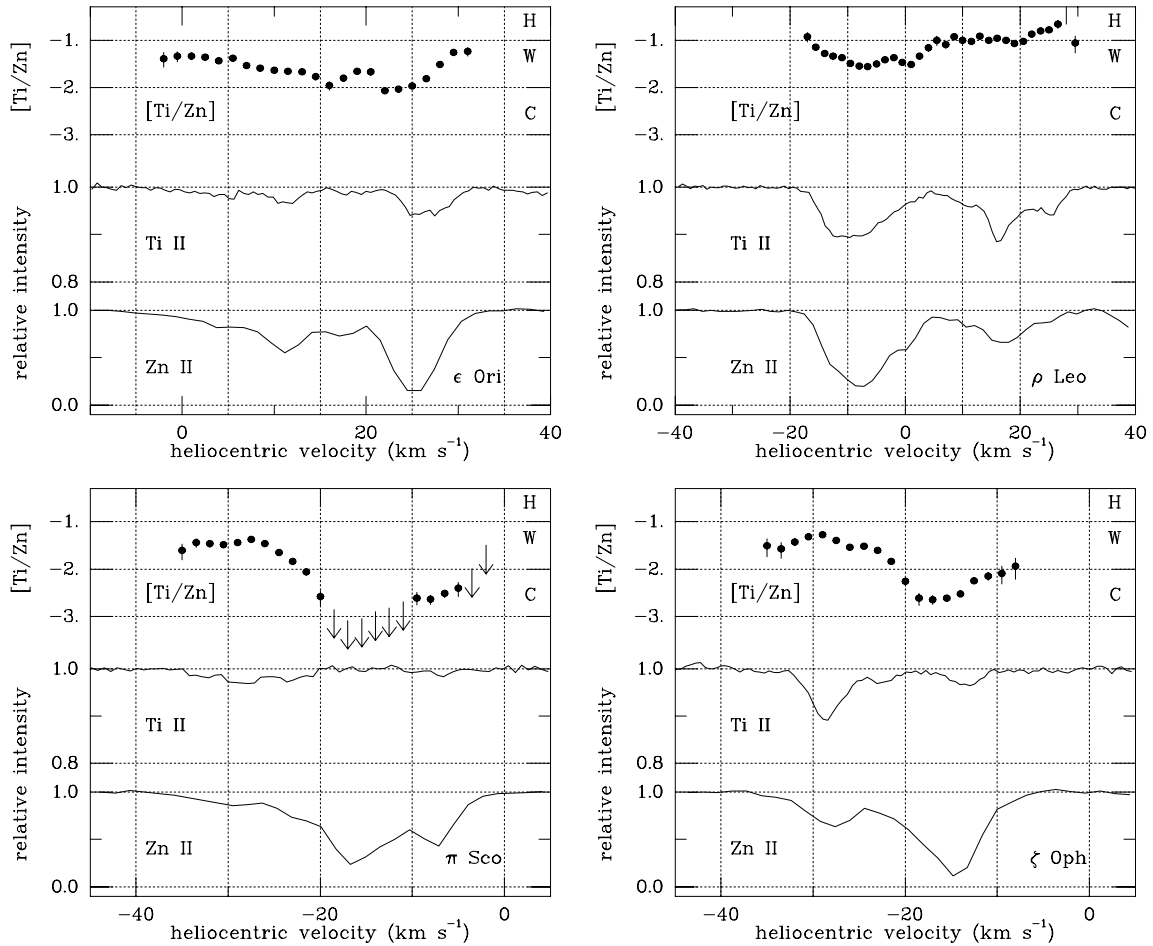
Figure 6. Spectra of Ti II (λ3383) and Zn II (λ2026 or λ2062) for four Galactic sight lines. The Ti II spectra are from the KPNO coudé feed (FWHM ~1.3–1.5 km s^{-1}); the Zn II spectra are from the *HST* GHRS (FWHM ~3.4–3.7 km s^{-1}). The points at the top of each panel show the relative abundance [Ti/Zn] (indicative of the titanium depletion), obtained from ratios of the 'apparent' optical depths, sampled at intervals of 1.5 km s^{-1}. Uncertainties in [Ti/Zn] are 1σ; limits are 3σ. The letters H, W, and C (at the upper right in each panel) give representative values for [Ti/Zn] for clouds in the low Galactic halo; warm, diffuse clouds in the disc; and colder, denser disc clouds.

suggest that D(Ti) ranges from −1.3 dex for the 'group A' components ($-36 \lesssim v \lesssim -25$ km s^{-1}; log[$N(H_{tot})$] ~ 19.6) to −3.1 dex for the 'group B' components ($-24 \lesssim v \lesssim -5$ km s^{-1}; log[$N(H_{tot})$] = 21.14), where the molecular material is located (e.g. Crawford et al. 1994). In many cases, the variations in [Ti/Zn] (and thus the titanium depletion) with velocity appear to be relatively smooth.

The [Ti/Zn] ratios in the three Magellanic Clouds sight lines in Fig. 7 also exhibit a variety of behaviours. Towards the LMC star Sk−67 5, most of the components identified in fits to the line profiles have rather similar [Ti/Zn] ratios, between about −0.8 and −1.3 dex. A much larger range in [Ti/Zn] – from about −0.3 to about −2.8 dex – is seen in the LMC2 region towards Sk−70 115, however. The most severe titanium depletion there is in the component at 220 km s^{-1}, where the bulk of the neutral atomic and molecular material is found (Tumlinson et al. 2002; Welty et al. 2006). Towards Sk 155 (in the SMC 'wing' region), [Ti/Zn] ranges over a factor of 20, from about −0.1 to −1.4 dex. The Ti depletions in the components between about 162 and 174 km s^{-1} are much less severe than would have been expected from the depletions found for Fe and Ni there – similar to (but not quite as extreme as) the remarkably mild depletions found for Si and Mg in those components (Welty et al. 2001 and in preparation; Sofia et al. 2006).

4 DISCUSSION

4.1 Differences in spatial distribution

In principle, differences in the ionization and/or depletion behaviour of the various species observed in the predominantly neutral (H I) gas may lead to corresponding differences in the distribution of those species, depending on specific environmental conditions. While some of those differences may be inferred from total sight line column densities, comparisons of the respective high-resolution absorption-line profiles can provide more direct indications of the degree to which those species coexist. With the notable exception of some of the sight lines in the Sco–Oph region (e.g. π Sco; Joseph & Jenkins 1991), the Ti II profiles shown in Figs. A1 and A2 most closely resemble those of Ca II and of various dominant ions of other significantly depleted elements (e.g. Fe II, Ni II), with the absorption often spread fairly smoothly over a relatively wide range in velocity. There is generally little sign of the distinct narrow components (with $b \lesssim 0.8$ km s^{-1}) seen for both Ca II and various trace neutral species (e.g. Na I, K I, Ca I) in spectra of comparable resolution – whether that narrow absorption is relatively weak (e.g. for some components seen towards ρ Leo and several of the stars in Orion) or very strong (e.g. for the main components seen towards
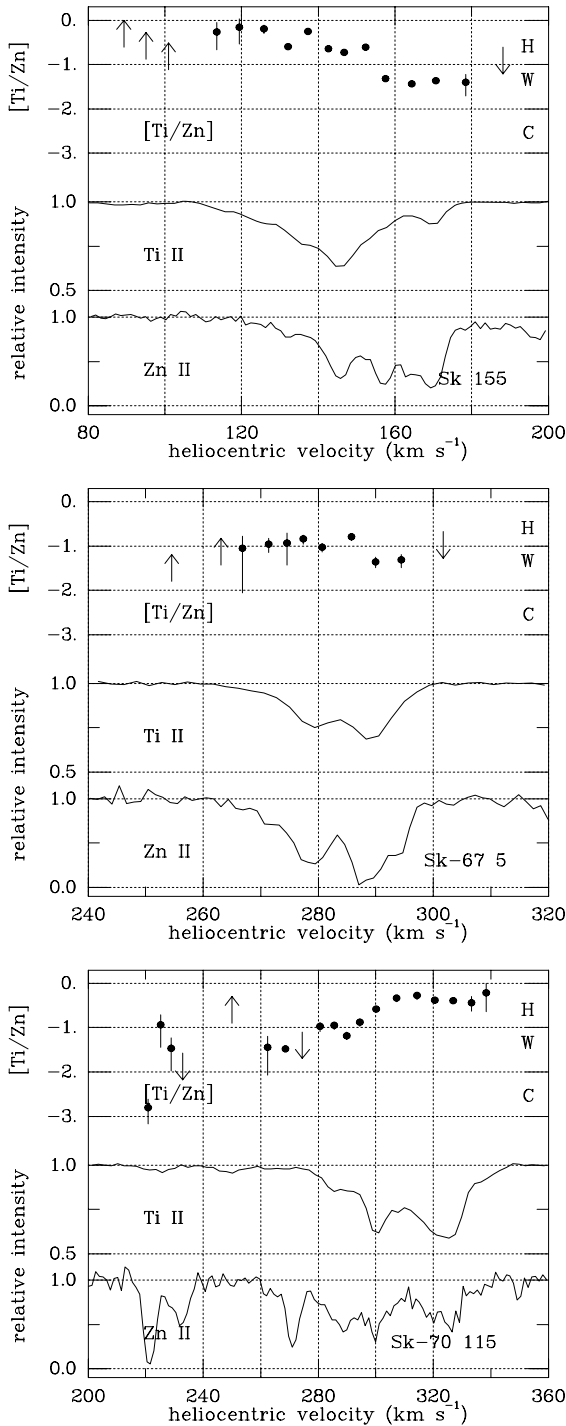
Figure 7. Spectra of Ti II (λ3383) and Zn II (λ2026) for one SMC sight line (Sk 155) and two LMC sight lines (Sk−67 5, Sk−70 115); only the Magellanic Clouds absorption is shown. The Ti II spectra are from UVES (FWHM $\sim$ 4.5 km s^{-1}); the Zn II spectra are from the *HST* STIS (FWHM $\sim$ 2.8 km s^{-1}). The points at the top of each panel show the relative abundance [Ti/Zn] (indicative of the titanium depletion), for components identified in simultaneous fits to the profiles of lines from many dominant species. Uncertainties in [Ti/Zn] are 1σ; limits are 3σ. The letters H, W and C (at the upper right in each panel) give representative values for [Ti/Zn] for clouds in the low Galactic halo; warm, diffuse clouds in the disc; and colder, denser disc clouds. The narrow absorption features in the Zn II spectrum of Sk−70 115 near 270 and 350 km s^{-1} are due to Mg I.

ζ Oph, χ Oph and other more heavily reddened stars). Fits to the Ti II profiles using component structures derived from Ca II often yield low Ti II/Ca II ratios for components with such small *b*-values (when *b* is well determined), and the Ti II absorption is often relatively weak for components with strong absorption from the trace neutral species – especially for components also detected in CH and CN. Offsets between the strongest Ti II absorption and the strongest molecular absorption are not uncommon – even when only lower resolution spectra are available. All these tendencies are consistent with the view that the observed Ti II absorption traces primarily the warmer, more diffuse gas – where the titanium depletions are much less severe than in the colder, denser clouds where the various trace neutral species and molecules are concentrated (e.g. Crinklaw et al. 1994). The absorption from Ca II traces both the colder, denser gas (where Ca II can be a dominant ion but calcium is severely depleted) and the warmer, more diffuse gas (where Ca II is a trace species but calcium is much less severely depleted) (Welty et al. 2003). The general decrease in the Ti II/Ca II ratio at higher column densities and/or higher $E(B − V)$ thus may primarily reflect changes in the calcium ionization balance (i.e. an increase in Ca II/Ca$_{tot}$) at higher average densities.

4.2 Depletions in individual components

Spitzer (1985) suggested that the correlations observed between the total sight line depletions of various elements and the mean sight line density $\langle n_H \rangle$ could arise if individual sight lines contained different proportions of moderate density 'standard' cold clouds, higher density 'large' cold clouds, and more smoothly distributed warmer, lower density neutral gas. Jenkins, Savage & Spitzer (1986) used that simple model, with the further assumption of constant depletions for each element in the cold and warm gas (more severe in the cold gas, less severe in the warm gas), to interpret a large body of abundance data derived from UV spectra obtained with *Copernicus* (with FWHM $\sim$ 15 km s^{-1}). More recent detailed studies based on higher resolution optical and UV spectra of individual sight lines (e.g. Fitzpatrick & Spitzer 1997; Welty et al. 1999b; Howk, Savage & Fabian 1999), however, suggest that there is a continuum of depletion behaviour in individual interstellar clouds – likely depending on both current physical conditions and past history – and that the commonly cited 'cold cloud', 'warm cloud' and 'halo cloud' depletion patterns (e.g. Savage & Sembach 1996) may be viewed as useful representative values within that continuum.

The [Ti/Zn] ratios shown in Figs 6 and 7, together with estimates of [Ti/Zn], [Ti/S] or [Ti/H] for individual components or component groups in additional sight lines, indicate that the titanium depletion may range (essentially continuously) from less than a factor of 2 to more than a factor of 3000 in individual interstellar clouds. The least severe Ti depletions [D(Ti) $\gtrsim$ −0.5 dex; assuming D(Zn) $\sim$ −0.1 dex] are found for several components towards the Galactic halo stars HD 93521 and HD 215733 (Albert 1983; Spitzer & Fitzpatrick 1993; Fitzpatrick & Spitzer 1997; Jenkins 2009) and for some of the components towards Sk 155 (SMC) and Sk−70 115 (LMC). The most severe Ti depletions [D(Ti) $\lesssim$ −3.0 dex; assuming D(Zn) $\sim$ −0.4 dex] are found for the main components ($-20 \lesssim v \lesssim -5$ km s^{-1}) towards ζ Oph, χ Oph, and several of the Sco-Oph stars; for the main components towards HD 62542 and several stars in the Taurus-Perseus region (ζ Per, HD 27778, X Per); and for the component near 220 km s^{-1} towards Sk−70 115 (LMC). These 'main' components typically contain most of the trace neutral

species and most of the molecular material in the respective lines of sight, and (presumably) arise in relatively cold, dense gas. Plots of the [Ti/Zn] ratios versus $N(\text{Zn\,II})$ reveal trends very similar to those seen for D(Ti) versus $N(H_{\text{tot}})$ (Fig. 3), but with slightly steeper slope.

Much of the scatter in Figs 3–5 is likely due to differences in the relative amounts of cold, moderately dense gas (with more severe depletions) and warmer, more diffuse gas (with milder depletions) for sight lines with similar overall $N(H_{\text{tot}})$, $E(B - V)$ or $f(H_2)$. A number of the sight lines with the least severe overall depletions, for a given $N(H_{\text{tot}})$ or $E(B - V)$, are quite complex – sampling either long paths dominated by relatively diffuse gas through the Galactic disc (or lower halo) or disturbed regions (e.g. near the Carina nebula; Walborn et al. 2002a) where significant dust processing has occurred. Conversely, a number of the sight lines with the most severe depletions are relatively nearby, with fewer components and a larger fraction of colder, denser gas. For example, the complex sight line towards HD 167971 [$d = 730$ pc, $E(B - V) = 1.08$, $N(H_2) = 7 \times 10^{20}$ cm^{-2}] has D(Ti) $= -2.32$ dex, while the much simpler sight line towards HD 27778 [$d = 225$ pc, $E(B - V) = 0.37$, $N(H_2) = 6.2 \times 10^{20}$ cm^{-2}] – with lower reddening but a higher molecular fraction – has D(Ti) $= -3.10$ dex. Severe depletions in a single component can easily be 'hidden' in overall average sight line values by much less severe depletions in other more diffuse components along the line of sight – even if those other components have lower aggregate $N(H_{\text{tot}})$.

4.3 Do depletions depend on local densities?

Both the observed correlations between the depletions of various refractory elements and the mean sight line density $\langle n_H \rangle$ (Fig. 2) and models of grain growth and destruction have suggested that the depletions in individual clouds should depend on the local hydrogen density n_H – but direct evidence for that dependence has been rather scanty. Estimates of n_H have recently been obtained for the main neutral components in a number of the sight lines in this Ti II survey, however. Where possible, Table 11 lists two values for the Ti depletions (for the sight line as a whole and for just the main neutral components) and two estimates for the local hydrogen densities. The first set of n_H is based on values of the thermal pressures ($n_H T$) derived from the fine-structure excitation of C I (Jenkins & Tripp 2001; Zsargó & Federman 2003; Welty et al. 2003) and the corresponding kinetic temperatures derived from the rotational excitation of H_2 (assuming the C I and H_2 to be coextensive); the second set of n_H (for more heavily reddened sight lines) was obtained from analyses of the rotational excitation of C_2 (van Dishoeck & Black 1982; Sonnentrucker et al. 2007). The two estimates for n_H are not directly comparable, as C_2 appears to trace somewhat denser, colder regions than C I and H_2 (e.g. Sonnentrucker et al. 2007). The Ti depletions in the main neutral components are generally estimated from the Ti II absorption over the velocity interval emcompassing the strongest components seen in Na I and/or K I, which are assumed to contain most of the total hydrogen, C I and C_2 in the sight line. These main component D(Ti) are typically factors of 2–3 more severe than the integrated sight line values.

For this rather small sample, there does not appear to be any clear relationship between D(Ti) (for the total sight line or for the main components) and either set of n_H, however. It is intriguing, for example, that the Ti depletions towards π Sco and ζ Oph are very similar (both overall and as functions of velocity) – even though the density and molecular fraction are much higher towards ζ Oph.

Table 11. D(Ti) vs. n_H

Star	D(Ti) all	D(Ti) main	n_H(C I) main	n_H(C$_2$) main	Ref
HD 23180	−2.86	–	45–70	265^{+335}_{-65}	1,2
HD 24398	−3.02	−3.3	10–16	215^{+285}_{-70}	1,2
HD 24534	−2.92	–	45–110	325^{+80}_{-80}	3,2
HD 24760	−2.26	−2.3	12–33	–	4
HD 27778	−3.10	–	–	280^{+35}_{-35}	2
HD 35149	−2.26	−2.3	10–16	–	1
HD 37742	−2.13	−2.2	16–40	–	1
HD 62542	−2.70	−3.0	–	500^{+570}_{-145}	2
HD 73882	−2.32	−2.7	–	520^{+745}_{-225}	2
HD 110432	−2.69	−3.1	–	140^{+35}_{-35}	2
HD 112244 A	−2.15	–	14–28	–	4
HD 112244 B	−2.15	–	17–48	–	4
HD 141637	−2.39	−2.8	200–800	–	4
HD 143018	−2.58	< −3.0	13–33	–	4
HD 144217	−2.69	−3.2	35–205	–	4
HD 147165	−2.74	−2.8	137–345	–	4
HD 147888	−2.97	−3.2	–	215^{+55}_{-30}	2
HD 148184	−2.68	−3.6	–	185^{+125}_{-30}	2
HD 149757	−2.62	−3.1	60–150	215^{+35}_{-35}	1,2
HD 154368	−2.49	−2.8	–	240^{+80}_{-40}	2
HD 206267	−2.37	–	40–95	315^{+125}_{-30}	3,2
HD 207198	−2.31	–	–	245^{+30}_{-60}	2
HD 210121	−2.28	−2.8	–	315^{+80}_{-80}	2

The first entry for D(Ti) is for the whole sight line; the second is for the 'main' component(s) – where the C I and/or C$_2$ are concentrated.
References for n_H: 1 = Welty et al. (2003); 2 = Sonnentrucker et al. (2007); 3 = this paper; 4 = Zsargó & Federman (2003).

Unfortunately, the estimates for the 'main component' depletion can be rather uncertain, as there could still be some warmer, more diffuse gas (with milder depletions) at velocities similar to those of the cooler gas traced by C I and C_2. Unresolved blends of gas with different properties may also affect the densities derived from C I (e.g. Jenkins & Tripp 2001), and the dynamic range sampled by the densities derived from C_2 excitation is not very large. More detailed component analyses of higher resolution spectra – to more reliably identify and characterize 'corresponding' components in Ti II, Zn II and C I – may yield a clearer picture of the relationship between D(Ti) and n_H.

4.4 Electron densities from Ca II/Ti II

Because Ca II is typically a trace ion in warmer, more diffuse clouds, the Ca II/Ti II ratio might, in principle, provide a useful measure of the electron density there (Stokes 1978) – if that ratio can be calibrated via independent determinations of n_e. Stokes & Hobbs (1976) derived the approximation

$$n_e \simeq \frac{\Gamma}{\alpha} \left[R \frac{N(\text{Ti\,II})}{N(\text{Ca\,II})} - 1 \right]^{-1}, \qquad (1)$$

where R, the ratio of the gas-phase abundances of Ca and Ti (in all ionization states), is assumed to not vary strongly and Γ/α is the ratio of the Ca II photoionization rate and the Ca III recombination rate coefficient. Stokes (1978) then estimated $R = 9.2 \pm 3.1$, using Ti II and Ca II column densities for the main component groups in 10

sight lines, together with values for n_e derived from the corresponding Ca I/Ca II ratios. Combining individual component Ti II column densities derived from the higher resolution spectra presented in this paper with corresponding values for Ca II and Ca I from Welty et al. (1996, 2003), for 19 components in seven sight lines, yields the same mean R but twice the standard deviation (the individual values for R range from 2 to 20). The differences in distribution of the three species complicate the calibration of R, as Ca I is detected primarily in the colder, denser gas (where the Ti II/Ca II ratio appears to be lower, on average, than in warmer, more diffuse clouds and where Ca II can be a dominant ion) and as the recombination rate coefficient α depends on the temperature. Moreover, estimates of n_e derived from Ca I/Ca II ratios are often significantly higher than values derived from other trace-dominant ratios (Welty et al. 2003) – so that R could be somewhat larger. Until these issues are resolved, values of n_e estimated from equation (1) must be considered to be very uncertain.

4.5 Scale height of Galactic Ti II absorption

Different constituents of the ISM can exhibit quite different distributions perpendicular to the Galactic plane – probing different levels of the Galactic halo and providing clues to the relationship between disc and halo gas. For example, while observations of Lyman α absorption suggest an exponential scale height of about 200 pc for neutral hydrogen (Diplas & Savage 1994), highly ionized species such as C IV and Si IV can extend much farther from the plane, with scale heights of order 3.5 kpc (e.g. Savage & Wakker 2009). Because the titanium depletion is typically less severe in more diffuse gas, the gas-phase Ti II/H I ratio would be expected to increase away from the Galactic plane (on average, as $\langle n_H \rangle$ decreases), so that observations of Ti II absorption might be used to trace the neutral material in the Galactic halo well beyond the 200 pc scale height of the H I. Based on Ti II detections towards 15 stars at distances $|z| \gtrsim 1$ kpc from the plane (and many stars below 1 kpc), Albert et al. (1994) concluded that the Ti II scale height could not yet be determined, but that it might be greater than 2–3 kpc. Lipman & Pettini (1995), however, using eight additional Ti II detections towards stars at $1.0 \lesssim |z| \lesssim 4.3$ kpc (plus four towards targets in the Magellanic Clouds), derived a scale height of 1.5 ± 0.2 kpc. Observations of the Galactic Ti II absorption towards 20 SMC and 34 LMC stars (Caulet & Newell 1996; Cox et al. 2006, 2007; this paper) yield $\log[N(\text{Ti II}) \sin|b|] = 11.74 \pm 0.13$ dex and 11.80 ± 0.10 dex, respectively – consistent with the values found by Lipman & Pettini (1995) – providing further support for a Ti II scale height $\lesssim 1.5$ kpc.

Lipman & Pettini (1995) also conjectured that titanium might be undepleted in the Galactic halo beyond $|z| \sim 1$ kpc. If gas in the low halo corotates with the disc, then towards the LMC its velocity would increase monotonically with $|z|$, reaching $v_\odot \sim 100$ km s^{-1} at $|z| \sim 7.5$ kpc; towards the SMC, the velocity of the gas would decrease out to $|z| \sim 4$ kpc, then increase steadily beyond that point (Savage & de Boer 1981). Given the non-zero dispersion in velocity for gas within the Galactic disc, identification of halo gas by velocity should thus be easier towards the LMC. The Ti II spectra of LMC targets in Fig. A2 all show absorption at $0 \lesssim v \lesssim 30$ km s^{-1}, due primarily to gas in the disc (with some contribution from gas in the low halo). For $40 \lesssim v \lesssim 100$ km s^{-1} (corresponding to gas at $3.5 \lesssim |z| \lesssim 7.5$ kpc), however, very little (if any) Ti II is detected, and it will be difficult to determine accurate titanium abundances. We note, however, that the relative abundances [X/Zn] (for X = Si, Cr, Mn, Fe and Ni) in the halo components

at $56 \lesssim v \lesssim 91$ km s^{-1} towards the LMC SN 1987A are consistent with no depletion of those refractory elements (Welty et al. 1999a).

4.6 D/H variations and deuterium depletions

In principle, the current abundance of deuterium (D/H) is dependent only on its initial ('primordial') abundance produced in the Big Bang (with a fairly sensitive dependence on the baryon density Ω_b) and its gradual destruction (via conversion to ^{3}He and ^{4}He) in subsequent generations of stars ('astration'). Measurements of the current local D/H ratio thus yield a firm lower limit to the primordial deuterium abundance (and a corresponding upper limit to Ω_b). If the actual primordial D abundance can be estimated independently, then the current D/H ratio may be used to constrain models of galactic chemical evolution (see, e.g. Pettini 2006; Steigman 2009; Linsky 2009 for recent summaries of some of these issues). The Galactic interstellar gas phase D I/H I ratio (which yields D/H directly if the molecular fraction is small and if there are no isotope-selective processes significantly affecting the ratio) has been measured towards $\sim$50 stars, at distances from 2.6 pc to 2.7 kpc and with N(H I) ranging from 4×10^{17} to 1.5×10^{21} cm^{-2} (as compiled by Linsky et al. 2006; Ellison et al. 2007; Lallement et al. 2008). The local D I/H I ratio appears to be roughly constant, at 15–16 ppm, for sight lines with N(H I) $\lesssim 1.5 \times 10^{19}$ cm^{-2} (mostly within 100 pc). There is considerable scatter in the ratio, however, along the more extended, higher N(H I) sight lines, where D I/H I ranges from 5 to 23 ppm; values of about 22 ppm have been measured in several clouds in the lower Galactic halo (Sembach et al. 2004; Savage et al. 2007). Measurements of the D I/H I ratio in a small number of low-metallicity damped Lyman α systems (where the effects of astration should be minimal) suggest that the primordial D/H ratio was about 28 ppm (Pettini et al. 2008, and references therein) – in excellent agreement with the predictions of standard Big Bang nucleosynthesis, as constrained by observations of the temperature fluctuations in the cosmic microwave background.

Several explanations for the scatter in the current Galactic D I/H I ratio have been proposed, with very different implications for Galactic chemical evolution: (1) The scatter in the D I/H I ratio could be due to localized infall and incomplete mixing of less processed material (with higher D/H ratios) – which would imply a relatively low 'true' current value for D/H, and thus significant astration. Observations of O I absorption along many of the same sight lines, however, do not reveal the anticorrelation between the O I/H I and D I/H I ratios that would be expected from differences in astration (e.g. Steigman, Romano & Tosi 2007). (2) Alternatively, the scatter in D I/H I could be due to variations in the selective depletion of deuterium into dust grains along the different lines of sight (Jura 1982; Tielens 1983; Draine 2006). In this case, the true current value for the D/H ratio would be at least as high as the highest observed value – which would imply fairly minimal astration.

If the scatter in the observed D I/H I ratios is due to variations in the depletion of the deuterium, we would expect to see correlations between the deuterium abundance and the abundances of other depleted species – as is generally the case for pairs of refractory elements in the Galactic ISM (e.g. Jenkins 2009). Such correlations have indeed been noted between D I/H I and Ti II/H I (Prochaska et al. 2005; Ellison et al. 2007; Lallement et al. 2008) and between D I/H I and Si II/H I and Fe II/H I (Linsky et al. 2006). The two low halo clouds with high D I/H I ratios also appear to be characterized by relatively mild depletions (Sembach et al. 2004; Savage et al. 2007). However, the sight line samples employed in those studies

are rather small, there are some sight lines which do not appear to follow the general trends, and the relative slopes of the correlations do not seem consistent with the known depletion behaviour of Si, Fe and Ti (Linsky et al. 2006; Ellison et al. 2007; Lallement et al. 2008).

In principle, several factors might contribute to the scatter in those relationships and/or to the apparently inconsistent correlation slopes (e.g. Linsky 2009):

(1) The presence of ionized gas in some of the sight lines with relatively low $N(H\,{\rm I})$ might account for some of the outliers in the relationships with Si and Fe (as Si II and Fe II would be present in the ionized gas, but not D I) and might contribute to some of the differences in the slopes of the relationships. Ionized gas should not affect the relationship between D I/H I and Ti II/H I, however, as both D I and Ti II should be present only in the neutral gas.

(2) As titanium is typically much more severely depleted than deuterium, different processes and/or sites may be involved in the depletions of the two elements, and the gas-phase Ti II/D I ratio may exhibit considerable variations. For example, if much of the Ti is locked in grain cores, but most of the D in more loosely bound mantles, there may be cases where much of the deuterium could be returned to the gas phase (e.g. via weak shocks) without significantly affecting the more tightly bound titanium. In principle, such a scenario could account for sight lines with high D I/H I but appreciable depletions of Ti (e.g. HD 41161, WD1034+001; Ellison et al. 2007); information regarding the depletions of other mildly depleted species in those sight lines would be valuable. On the other hand, subsequent destruction of the grain cores could significantly increase the gas-phase Ti without much increase in the gas-phase D.

(3) Many of the sight lines exhibit complex component structure in the available high-resolution optical/UV spectra, and there may be cases where the gas-phase D and Ti are distributed very differently among the various components (e.g. Prochaska et al. 2005). The sight line towards μ Col, for example, appears to be somewhat anomalous, with low D I/H I but mild overall Ti depletion (Ellison et al. 2007; Lallement et al. 2008). Examination of the profiles of both mildly and severely depleted species suggests that the bulk of the hydrogen (and presumably D) is in the components between about 10 and 35 km s^{-1}, while the more refractory species (including Ti) have significant contributions from the component near 40 km s^{-1} – which has a relatively low $N(H_{\rm tot})$ but very mild depletions (e.g. Howk et al. 1999; Lallement et al. 2008). If only the lower velocity components are considered, then the μ Col sight line would not be as discrepant.

(4) The current relatively small sample of sight lines with data for both D I and Ti II is not representative of the larger set of Galactic sight lines for which the Ti depletion is known. For the small D-Ti sample, plots of D(Ti) versus both $N(H_{\rm tot})$ (as in Fig. 3) and the mean sight line density $\langle n_{\rm H} \rangle$ (e.g. fig. 5 in Ellison et al. 2007) indicate that the higher $N(H_{\rm tot})$ sight lines (all towards fairly distant stars) are all characterized by milder than average Ti depletions – so that the slopes in each case are much shallower than those seen for the full Galactic Ti II sample. There appear to be no sight lines with detections of D I for which D(Ti) is less than −2 dex.

(5) The steeper than expected slopes of relationships involving the Si depletion (in the small D-Si sample) are strongly influenced by the rather uncertain data point for θ Car, which has the most severe Si depletion in the sample (e.g. fig. 5 in Ellison et al. 2007). The Si II column density for θ Car is taken from the *Copernicus* study of Allen, Jenkins & Snow (1992), who ascribed about 70 per cent of the observed Si II to an ionized component in that sight line – but the various other first ions (e.g. C II, Mg II, S II, Fe II) were all assigned entirely to the neutral component. Increasing the Si II column density for θ Car by a factor of 2–3 would make the D-Si sample more consistent with the larger Galactic Si II sample.

Observations of Ti II in the rest of the sight lines of the D I sample – to increase the size of the D-Ti sample and minimize ionization effects – should provide a clearer test of the deuterium depletion hypothesis. In view of the observed trend in D(Ti) versus $N(H_{\rm tot})$ (Fig. 3), Ti II may well be detectable even at the low hydrogen column densities characterizing some of those sight lines.

4.7 Ti II in the Magellanic Clouds

A primary motivation for studies of the interstellar Ti II absorption in the Magellanic Clouds is to explore the behaviour of elemental depletions and dust properties in lower metallicity galaxies – i.e. to see whether the patterns and levels of depletion and/or the composition of the dust vary with metallicity. The Magellanic Clouds are particularly useful for such studies because the total interstellar (gas plus dust) abundances of many elements may be inferred from analyses of the abundances in stellar atmospheres (for a variety of stellar types) and in gaseous nebulae at many locations within the two galaxies. The current overall metallicities are sub-solar by factors of about 2 in the LMC and 4–5 in the SMC (except for C and N, which are somewhat more deficient). The *relative* elemental abundances, however, are generally fairly similar to those found locally in our Galaxy (within the typical 0.1–0.2 dex uncertainties) – at least for most of the elements commonly detected in the ISM (e.g. Russell & Dopita 1992; appendices in Welty et al. 1997, 1999a). For example, the current Ti/Fe ratios (in relatively young stars) are about −2.44 dex in the LMC and −2.49 dex in the SMC, versus −2.55 dex in the solar photosphere (Lodders 2003). For predominantly neutral clouds in the SMC and LMC, depletions may thus be estimated by taking ratios of the column densities of the dominant ions of various refractory elements with respect to $N(S\,{\rm II})$ and/or $N(Zn\,{\rm II})$ (which are typically at most very mildly depleted) and comparing with the corresponding stellar/nebular ratios – and those relative abundances may be fairly directly compared with Galactic values.

Although detailed interstellar abundance data are available for only a few sight lines in the Magellanic Clouds, there are some intriguing indications of differences in the depletion patterns, particularly for Si, Mg and Ti in the SMC. In several of the main components towards Sk 155, for example, ratios of the column densities of Si II, Mg II and Ti II with respect to those of Zn II and S II (as for the [Ti/Zn] in Fig. 7) indicate that all three of those elements are much less severely depleted than would have been expected from the significant depletions of Fe and Ni in those components – a pattern not seen (to this point) in any Galactic sight line (Welty et al. 2001 and in preparation; cf. Sofia et al. 2006). Milder than expected depletions of Si and Mg are also seen in the component at 220 km s^{-1} towards the LMC star Sk−70 115 (Welty et al. 2004 and in preparation) – but in that case Ti is severely depleted (Fig. 7), consistent with the severe depletion of Fe in that component. These differences in depletion patterns are most easily seen in components with fairly severe depletions of at least some of the more refractory elements. Unfortunately, few such components have been identified in the Magellanic Clouds; additional UV spectra of more reddened LMC and SMC sight lines are needed to gauge the prevalence of any 'anomalous' depletions. Because titanium is not a major

constituent of the dust, any differences in the pattern of Ti depletion would primarily affect its utility as a depletion indicator. If the very mild depletions of Si and Mg seen towards Sk 155 (and several other SMC stars) are typical of the SMC, however, there would be significant implications for the composition of the dust there, as most models for SMC dust rely heavily on silicates (and require most of the available silicon) (e.g. Cartledge et al. 2005; Li, Misselt & Wang 2006).

4.7.1 Line profiles and Ti II/Ca II ratios

The Ti II data now available for the Milky Way, SMC and LMC reveal both similarities and differences in the behaviour of titanium in the interstellar media of the three galaxies. As in the Galactic ISM, the Ti II profiles in the Magellanic Clouds typically are relatively smooth and spread over a fairly wide velocity range – more similar to the corresponding profiles of Ca II (and those of other dominant ions of depleted elements) than to the narrower, more structured profiles of Na I, K I, or the various molecular species (Cox et al. 2006, 2007; Welty et al. 2006; Welty & Crowther, in preparation). The absorption from both Ti II and Ca II often is much stronger, relative to that of Na I, in the Magellanic Clouds. The variations in the Ti II/Ca II ratio are again fairly smooth with velocity in the SMC and LMC, but the ratio itself is typically larger – both for individual velocity components (or velocity intervals) and for the integrated sight line values – which may be due to enhanced ionization of the Ca II in the (generally) stronger radiation fields there. There are, however, still cases of low Ti II/Ca II ratios in both the SMC and LMC, such as in the highest velocity components towards stars at the southwestern end of the main 'bar' of the SMC (e.g. Sk 40, AV 47) and in the components near $220\,\mathrm{km\,s^{-1}}$ towards Sk−70 115 in the LMC2 region.

4.7.2 Ti II depletions

The most striking difference in the behaviour of titanium in the three galaxies is the much milder Ti depletion, for any given $N(H_{\mathrm{tot}})$, $E(B-V)$ or $f(H_2)$, in the LMC and (especially) the SMC (Figs 3–5). Because the depletions are computed with reference to the stellar titanium abundances in each galaxy, the D(Ti) in each case represent the fraction of Ti in the gas phase, relative to the total amount of titanium available (which is lower in the LMC and SMC; Table 10). In nearly all the sight lines (Galactic, LMC and SMC), the H I column densities have been derived from fits to the damped Lyman α absorption profiles (not from 21-cm emission profiles), over the same path as the Ti II absorption. In addition, the molecular fractions are typically fairly small in the SMC and LMC – so that $N(H_{\mathrm{tot}})$ is generally not much greater than $N(H\,I)$. The higher gas-phase abundances of titanium (and inferred milder Ti depletions) in the Magellanic Clouds thus are not due either to higher overall titanium abundances or to significantly underestimated total hydrogen column densities [even where $N(H_2)$ is not known].

One factor which might contribute to differences in the overall level of the integrated sight line depletions in the Milky Way, LMC and SMC is the ratio of cold, dense gas (with more severe depletions) to warmer, more diffuse gas (with milder depletions) sampled in each galaxy [as discussed above regarding the scatter in D(Ti) at any given $N(H_{\mathrm{tot}})$ within each of the three galaxies]. Wong et al. (2009) have recently conjectured, for example, that regions in the LMC with high H I column densities but no associated CO emission might be characterized by a higher fraction of warm, diffuse gas. Most of the

Galactic sight lines in the current sample lie primarily within the disc, where the colder, denser gas is more likely to be found. The sight lines that probe significant lengths through the Galactic halo generally exhibit less severe overall depletions than the average Galactic value [at any given $N(H_{\mathrm{tot}})$]. The Milky Way portion of the absorption towards the Magellanic Clouds targets, for example, has $N(H) \sim 4 \times 10^{20}\ \mathrm{cm^{-2}}$ (SMC) or 4–$8 \times 10^{20}\ \mathrm{cm^{-2}}$ (LMC) (estimated from 21-cm emission profiles; e.g. Staveley-Smith et al. 2003), with an average D(Ti) ~ -1.6 dex – very similar to the values seen towards Galactic halo stars at $|z| \gtrsim 1$ kpc (e.g. Lipman & Pettini 1995). The Magellanic Clouds sight lines, however, all probe gas in the outer 'halo' regions of the LMC or SMC, with (perhaps) some contribution from gas in the main body of the galaxy (depending on the location of the target star within the galaxy). Many of the targets in runs V02 and V04, for example, were chosen to be relatively lightly reddened, and may thus lie preferentially in front of much of the interstellar material in the SMC and LMC along those sight lines. For a number of the LMC sight lines, for example, fits to the Lyman α absorption profiles yield only upper limits for LMC $N(H\,I)$ (Table 9; Welty, in preparation), and little, if any, Na I is detected (Fig. A2).

Differences in the ratios of cold, dense gas to warm, diffuse gas probably cannot entirely account for the observed differences in Ti depletions among the three galaxies, however. Most of the SMC and LMC sight lines observed in runs V01 and V03, for example, exhibit significant column densities of Na I and/or H_2 (Tumlinson et al. 2002; Welty et al. 2006; Welty & Crowther, in preparation); several have detections of CN and/or CO absorption (André et al. 2004; Welty et al. 2006). Such sight lines presumably probe appreciable amounts of colder, denser gas in the Magellanic Clouds, as the kinetic temperatures inferred from the H_2 rotational excitation are similar to those found for Galactic sight lines with comparable $N(H_2)$ (Tumlinson et al. 2002; Cartledge et al. 2005). Even those sight lines, however, generally exhibit significantly milder Ti depletions than those found for Galactic sight lines with comparable $N(H_{\mathrm{tot}})$ and $f(H_2)$. Towards Sk 143 (SMC), with $\log[N(CN)] = 12.47$ and $\log[N(CH) = 13.60$ (Welty et al. 2006), D(Ti) $= -1.68$ dex for the sight line as a whole – versus -2.0 to -3.1 dex for Galactic sight lines with similar column densities of CN or CH. If most of the SMC $N(H_{\mathrm{tot}})$ towards Sk 143 is assumed to be in the component near $133\,\mathrm{km\,s^{-1}}$ (which contains the CH, CN and most of the Na I), then D(Ti) in that main component would be of order -2.3 dex – again less severe than for comparable individual Galactic components. As noted above, however, Ti is severely depleted ([Ti/Zn] ~ -2.8 dex) in the main component(s) towards Sk−70 115 (LMC).

4.7.3 Depletions and local densities

While no clear relationship was discerned between the Ti depletion and the local hydrogen density in the Galactic sight lines, it is still worth examining corresponding data for the Magellanic Clouds. Analyses of the C I fine-structure excitation, in the handful of Magellanic Clouds sight lines with suitable UV spectra, indicate that the thermal pressures ($n_H T$) in the main LMC or SMC components appear to be factors of 4–5 higher than those typically found in the local Galactic ISM (e.g. Jenkins & Tripp 2001; André et al. 2004; Welty et al., in preparation). Such elevated pressures are consistent with theoretical models of interstellar clouds (e.g. Wolfire et al. 1995), which predict that higher pressures are needed to obtain stable cold, neutral clouds in environments characterized by

lower dust-to-gas ratios and stronger ambient radiation fields. As the kinetic temperatures inferred from analyses of the H_2 rotational excitation in those sight lines (50–80 K; Tumlinson et al. 2002; Welty et al., in preparation) are generally similar to those found in Galactic sight lines, the local hydrogen densities in the main LMC and SMC components would thus be *higher* than those in otherwise comparable Galactic clouds. The milder Ti depletions in the LMC and SMC thus apparently cannot be ascribed to generally lower local hydrogen densities there.

4.8 Intermediate-velocity gas towards the LMC

While the absorption seen for many neutral and ionized species at $v \lesssim 100 \, \mathrm{km \, s^{-1}}$ and at $v \gtrsim 200 \, \mathrm{km \, s^{-1}}$ towards the LMC may be reasonably ascribed to gas in the Milky Way (disc and halo) and in the LMC, respectively, the origin of the absorption seen at intermediate velocities has been somewhat controversial (de Boer, Morras & Bajaja 1990; Staveley-Smith et al. 2003). This intermediate-velocity (IV) absorption is commonly seen for Ca II and in the stronger lines of the dominant ions (in either neutral or somewhat ionized gas) of various abundant elements (e.g. Si II, Fe II), but is seldom seen for trace neutral species or H_2 (Savage & de Boer 1981; Wayte 1990; Welty et al. 1999a; Danforth et al. 2002; Tumlinson et al. 2002; Welty & Crowther, in preparation).

Lehner et al. (2009) have analyzed sensitive H I 21-cm emission spectra together with far-UV spectra obtained with *FUSE* in order to characterize the depletions and physical properties of this IV gas. They detect H I emission in about one-third of the 139 LMC sight lines examined, with $N(\mathrm{H\,I})$ ranging from about $2.5–16 \times 10^{18}$ cm^{-2}, and absorption from O I and/or Fe II in more than two-thirds of the sight lines. The column density ratios O I/H I and O I/Fe II suggest that the gas has a metallicity of about one-third solar and is predominantly ionized; the relative abundances of Si II, S II and Fe II suggest that some dust may be present. Some highly ionized gas, traced by O VI, is found in most of the sight lines. Lehner et al. conclude that the IV gas is associated with the LMC.

Intermediate-velocity absorption from Ca II is detected for all the LMC sight lines in Table 6 (most of which are included in the Lehner et al. 2009 sample); Ti II is detected in a few cases. The Ti II/Ca II ratios in the IV gas range from about 0.1 to 0.5 – somewhat lower than the values typical of the main LMC gas at $v \gtrsim 200 \, \mathrm{km \, s^{-1}}$. The Ti II/H I and Ti II/O I ratios (for which ionization corrections should be minimal) indicate very mild Ti depletions, of order -0.5 to -0.1 dex; slightly larger Ti II deficits relative to Fe II are consistent with the gas being predominantly ionized. Very mild depletions, similar to those found for Galactic halo clouds, also were found for Mg, Al, Si, Cr, Mn, Fe and Ni in the IV gas towards SN 1987A (Welty et al. 1999a).

4.9 QSO absorption-line systems

Measurements of the gas-phase abundances of various atomic species in the absorption-line systems seen towards distant quasars and gamma-ray bursts – primarily the damped and sub-damped Lyman α systems, with $\log N(\mathrm{H/I}) \geq 20.3$ and from 19.0 to 20.3, respectively – provide a key avenue for understanding the build-up of heavy elements and dust in galaxies, over a substantial fraction of the age of the Universe. The mean metallicities inferred from large samples of damped Lyman α systems (DLAs), over the redshift interval $0.1 \lesssim z \lesssim 5$, indicate (1) systematically lower values than those expected from models of galaxy evolution and other indications of star formation, (2) only modest evolution (slope $\sim$

-0.25 dex per unit redshift) and (3) a significantly subsolar value at the lowest redshifts (e.g. Prochaska et al. 2003b; Kulkarni et al. 2005). While a small number of 'metal-rich' DLAs have been identified (e.g. Herbert-Fort et al. 2006), a significant fraction of the 'missing' metals may be in the sub-DLAs, which have both systematically higher mean metallicities than the DLAs and roughly solar mean metallicities at low z – at least for the current relatively small sub-DLA sample at $z \lesssim 3.2$ (e.g. Khare et al. 2007; Kulkarni et al. 2007; Meiring et al. 2008; Péroux et al. 2008; Dessauges-Zavadsky, Ellison & Murphy 2009).

Attempts to determine the nucleosynthetic history of the galaxies traced by the DLAs and sub-DLAs – e.g. gauging the relative contributions of Type I and Type II supernovae by examining the relative gas-phase abundances of the so-called α and Fe-peak elements – have been complicated by the generally poorly known effects of depletion, which can yield abundance ratios for some elements that are similar to those seen in the Galactic metal-poor stars that exemplify the Type II-dominated abundance pattern (e.g. Lauroesch et al. 1996; Lu et al. 1996; Prochaska & Wolfe 2002; Vladilo 2002; Dessauges-Zavadsky et al. 2004). Positive values of the [Si/Fe] ratio, for example, could be consistent either with solar total abundances and some degree of depletion or with a Type II abundance pattern (with enhancements of the α-elements Mg, Si, S, etc.) and no depletion. Attempts to assess and correct for the effects of depletion (e.g. Vladilo 2002, 2004; Dessauges-Zavadsky et al. 2002, 2004; Jenkins 2009) generally assume that the depletion patterns in the absorbers are the same as those found in the Galactic ISM – i.e. that the composition of the dust is independent of metallicity (or any other factors that may be different in the absorbers). In view of the ambiguities in the interpretation of some of the more readily determinable ratios (e.g. Si/Fe), attention has been given to ratios such as Ti/Fe and Mn/Fe, where the effects of Galactic depletion and Galactic nucleosynthetic history act in opposition (e.g. Ledoux et al. 2002; Dessauges-Zavadsky et al. 2002). Because Ti (a Type II product) is generally more severely depleted than Fe (primarily a Type I product) in the Galactic ISM, positive values of [Ti/Fe] would be suggestive of an underlying type II abundance pattern (and negligible depletion), while negative values of [Ti/Fe] could be more consistent with solar total abundances and some degree of depletion. The differences in the depletions of Mg, Si and Ti found in some SMC and LMC sight lines suggest, however, that corrections for dust based on Galactic depletion patterns might not be appropriate, given the lower metallicities characterizing most of the higher-z absorbers – especially as LMC- or SMC-like UV extinction curves have typically been inferred for those systems (e.g. Pei, Fall & Bechtold 1991; Wild, Hewett & Pettini 2006; York et al. 2006; Vladilo, Prochaska & Wolfe 2008).

While the number of DLAs and sub-DLAs with detections of Ti II absorption is still relatively small, some preliminary comparisons can be made between the behaviour of Ti II in the absorbers, in our Galaxy and in the Magellanic Clouds. Table A3 lists 79 absorption line systems for which Ti II column densities (35 detections, 44 limits) have been published, together with column densities for H I, H_2, Zn II and Ca II. Where possible, the table also lists values for [Zn/H] (an indicator of the metallicity) and for [Ti/Zn] (an indicator of the Ti depletion). (While [Ti/Zn] will underestimate the severity of the depletion if the α-elements are enhanced in any particular system, such differences would be expected to be less than factors of 2–3, in view of the [Ti/Zn] ratios seen for Galactic metal-poor stars at comparable metallicities.) For this sample, the system redshifts range from 0.43 to 3.77; the H I column densities range from $<10^{18.8}$ to $10^{21.9}$ cm^{-2} (38 of the systems are DLAs, 19 are sub-DLAs); the
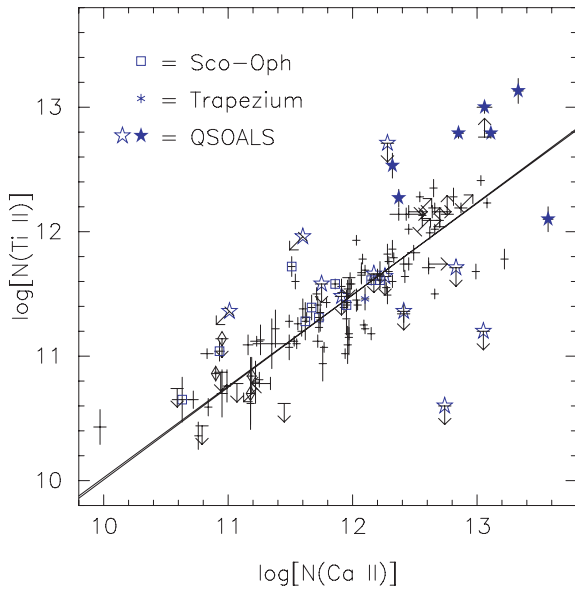
Figure 8. $N(\text{Ti}\,\textsc{ii})$ vs. $N(\text{Ca}\,\textsc{ii})$ for both Galactic sight lines and QSO absorption-line systems. Blue stars denote QSO absorbers (filled symbols for detections, open symbols for limits); blue open squares denote Sco-Oph sight lines; blue asterisks denote Orion Trapezium region sight lines; plus signs denote other Galactic sight lines (with size indicating $\pm 1\sigma$ uncertainties). The two (nearly indistinguishable) solid lines, with slopes ~ 0.7, represent weighted and unweighted fits to the Galactic data (not including the Sco-Oph or Trapezium sight lines).

Figure 9. Titanium depletions – D(Ti) for Galactic sight lines and [Ti/Zn] for QSO absorption-line systems – vs. $N(H_{\text{tot}})$. Blue stars denote QSO absorbers (filled symbols for detections, open symbols for limits); blue open squares denote Sco-Oph sight lines; blue asterisks denote Orion Trapezium region sight lines; plus signs denote other Galactic sight lines (with size indicating $\pm 1\sigma$ uncertainties). The depletions are relative to the solar Ti abundance in our Galaxy and relative to the observed zinc abundance in the QSO absorbers (assuming that zinc is undepleted). The two solid lines, with slopes ~ -0.65, represent weighted and unweighted fits to the Galactic data (not including the Sco-Oph or Trapezium sight lines).

metallicities (as gauged from [Zn/H]) range from about -1.6 to $+0.7$ dex.

Fig. 8 shows the relationship between $N(\text{Ti}\,\textsc{ii})$ and $N(\text{Ca}\,\textsc{ii})$ for the QSO absorbers (filled or open stars), with the Galactic data and trend lines also shown for reference (as in Fig. 1). While only seven of the absorbers have detections of both Ti II and Ca II, six of those lie above the general Galactic relationship, in the region occupied by the LMC and SMC sight lines; the seventh absorber (and four others with upper limits for Ti II), however, lie well below the Galactic trend. The Ti II and Ca II column densities derived from composite low-resolution Sloan Digital Sky Survey spectra of 27 systems selected for detectable Mg II, Ca II and Zn II (Wild et al. 2006; see last three entries of Table A3) and of larger numbers of systems selected for various other properties (York et al. 2006; see their table A4) also lie somewhat above the Galactic trend. Where both Ti II and Ca II are detected, the [Ti/Zn] ratios suggest very mild Ti depletions ([Ti/Zn] $\gtrsim -0.7$ dex); the four absorbers with upper limits on Ti II that lie significantly below the Galactic trend, however, all exhibit more severe Ti depletions ([Ti/Zn] $\lesssim -1.3$ dex).

Fig. 9 shows the relationship between D(Ti) and $N(H_{\text{tot}})$ for the absorbers, again with the Galactic data and trend lines for comparison (as in Fig. 3). Although there is considerable scatter in D(Ti) at any $N(H_{\text{tot}})$, most of the absorber data lie well above the region occupied by the Galactic sight lines, in many cases at slightly higher (less negative) D(Ti) and somewhat lower $N(H_{\text{tot}})$ than the SMC sight lines. All the absorbers with $\log[N(H_{\text{tot}})] < 20.3$ and D(Ti) < -0.9 dex – which overlap with the lower column density end of the Galactic distribution – are metal-rich sub-DLAs, with [Zn/H] ranging from 0.0 to $+0.7$ dex. The rest of the absorbers exhibit a range in metallicity ([Zn/H]) for any given D(Ti) or $N(H_{\text{tot}})$; there may be a tendency for lower metallicities at higher $N(H_{\text{tot}})$, as seen for the sub-DLAs and DLAs in general (e.g. Khare et al. 2007). While the data for the Milky Way, LMC and SMC (Fig. 3) suggest
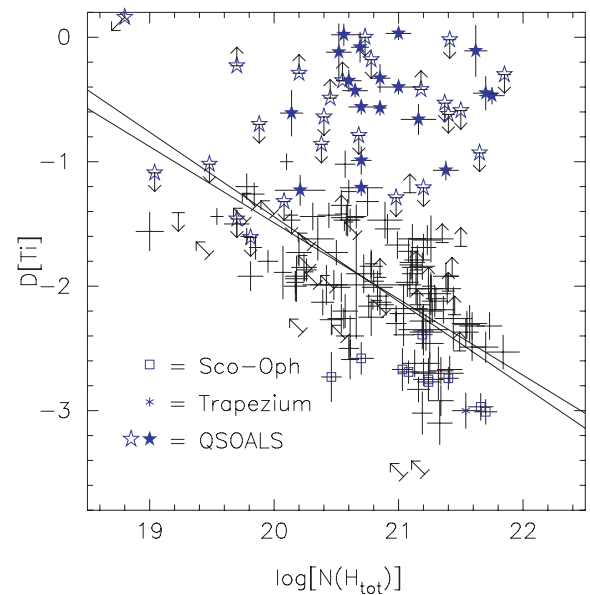
trends of increasingly severe Ti depletion at higher $N(H_{\text{tot}})$ for sight lines within any individual system (at some constant metallicity), the ensemble of QSO absorbers (single sight lines through systems spanning a range of metallicities) in Fig. 9 exhibits generally less severe Ti depletions at higher $N(H_{\text{tot}})$ – a consequence of trends for (1) lower metallicities at higher $N(H_{\text{tot}})$ and (2) more severe depletions (on average) at higher metallicities (see next).

Fig. 10 shows the relationship between D(Ti) and metallicity (which is assumed to be 0.0 dex for the Galactic sight lines, -0.3 dex for the LMC sight lines, -0.7 dex for the SMC sight lines and [Zn/H] for the DLAs and sub-DLAs). The uncertainties on the metallicity are arbitrarily assumed to be 0.1 dex for the Galactic, LMC and SMC sight lines – to give a rough indication of the density of points as a function of D(Ti). As noted in previous studies of DLA abundances (e.g. Ledoux, Petitjean & Srianand 2003; Noterdaeme et al. 2008), there appears to be a trend of increasingly severe depletion at higher metallicities – which is not due to the presence of the Zn II column density in both quantities, as the uncertainties in $N(\text{Zn}\,\textsc{ii})$ are generally less than 0.2 dex. In the metallicity range from -0.7 to 0.0 dex, the QSO absorbers generally exhibit somewhat milder Ti depletions than the SMC, LMC and Milky Way – perhaps an indication that most of the absorber sight lines contain a larger fraction of warm, diffuse gas (as might be expected on cross-section considerations). Given the lower metallicities characterizing most DLAs at $z \gtrsim 1.6$, Kanekar et al. (2009) conclude that those higher-z DLAs are dominated by warm gas, based on an apparent anti-correlation between metallicity and the spin temperature derived from observations of 21-cm absorption. The two absorbers in this sample with known significant column densities of H_2 [F0812+32 ($z = 2.6263$) and Q1331 + 170 ($z = 1.7765$)] both
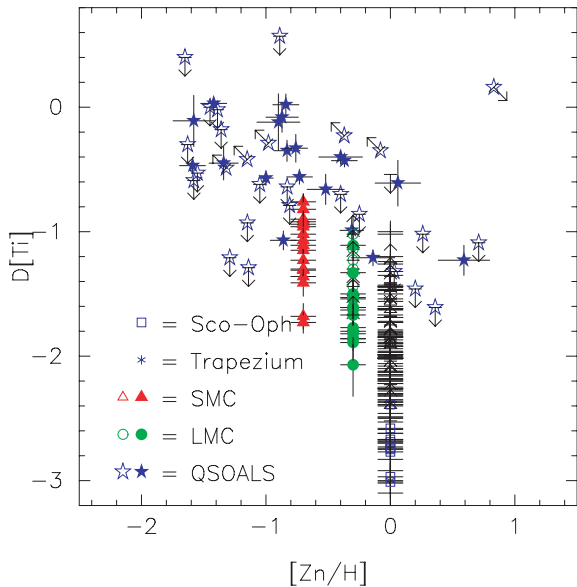
Figure 10. Titanium depletions – D(Ti) for Galactic sight lines and [Ti/Zn] for QSO absorption-line systems – vs. metallicity – 0.0 for Milky Way, −0.3 for LMC, −0.7 for SMC, [Zn/H] for QSO absorbers. Blue stars denote QSO absorbers, green circles denote LMC sight lines, red triangles denote SMC sight lines (filled symbols for detections, open symbols for limits); blue open squares denote Sco-Oph sight lines; blue asterisks denote Orion Trapezium region sight lines; plus signs denote other Galactic sight lines (with size indicating $\pm 1\sigma$ uncertainties; 0.1 dex assumed for Galactic, LMC, SMC metallicities). The depletions are relative to the solar Ti abundance in our Galaxy and relative to the observed zinc abundance in the QSO absorbers (assuming that zinc is undepleted).

have more severe Ti depletions than those seen for other systems at comparable metallicities – consistent with the general trend for systems with higher $f(H_2)$ (e.g. Noterdaeme et al. 2008). While the subset of absorbers with strong Ca II absorption is characterized by a higher dust content (reddening) than the general absorber population (e.g. Wild & Hewett 2005), there is no apparent trend in the severity of Ti depletion with $N(Ca II)$ (see also Nestor et al. 2008).

5 SUMMARY/CONCLUSIONS

We have combined several new sets of absorption-line data for interstellar Ti II (for 60 sight lines in our Galaxy and 43 sight lines in the lower metallicity Magellanic Clouds) with previously reported data for Ti II and other atomic and molecular species, in order to explore the behaviour of Ti II in a wide variety of interstellar environments. The new data include (most of) the highest resolution Ti II spectra yet reported (FWHM $\sim$ 1.3–1.5 km s^{-1}, for 17 of the Galactic sight lines), a significantly expanded sample of Ti II spectra for more heavily reddened Galactic sight lines (29 with $E(B - V) \geq 0.35$), and the most extensive set of Ti II spectra obtained for sight lines in the Magellanic Clouds (15 in the SMC, 28 in the LMC).

Comparisons of the highest resolution Galactic Ti II spectra with corresponding high-resolution spectra of Na I, K I and Ca II directly reveal differences in the distribution of those species – which reflect differences in their ionization and depletion behaviour and in the physical properties of the various interstellar clouds probed. In general, the Ti II profiles are relatively smoothly varying, and resemble

most the profiles seen for Ca II and for the dominant ions of various other refractory elements – with little indication of the narrow absorption components (likely due to relatively cold, moderately dense gas) seen for both Ca II and various trace neutral species. Both the line profiles and the Ti II column densities – obtained from detailed fits to the line profiles and/or by integrating the 'apparent' optical depths over the line profiles – suggest that the observed gas-phase Ti II traces primarily the warmer, more diffuse gas, and that Ti is severely depleted into the dust in the colder, denser clouds where the trace neutral and molecular species are most abundant. The total Galactic (disc plus halo) Ti II column densities towards stars in the Magellanic Clouds are consistent with a Galactic Ti II scale height $\lesssim 1500$ pc.

The Galactic column densities of Ti II and Ca II are well correlated, with $N(Ti II)$ varying roughly as $N(Ca II)^{0.7}$. The two species also appear to be fairly well correlated in the SMC and LMC, but the slope of the relationship is somewhat steeper and the average Ti II/Ca II ratio is somewhat higher (for the current sample of sight lines). Variations in the Ti II/Ca II ratio may reflect differences in the relative depletions of Ti and Ca and/or changes in the calcium ionization balance. While the Ca II/Ti II ratio might (in principle) be used to estimate the electron density in diffuse clouds where Ca II is a trace ion, calibration of that ratio is complicated by differences in the spatial distributions of Ca I, Ca II and Ti II and by differences in the temperature and calcium ionization balance between the diffuse clouds and the denser clouds where Ca I is detected.

In the currently available sample of Galactic sight lines, the titanium depletion ranges from about −1.0 dex (towards the low halo star HD 93521) to about −3.1 dex (towards the moderately reddened HD 27778). The depletions in individual components or small velocity intervals [gauged via reference to high-resolution UV spectra of Zn II and/or by assuming that most of the total $N(H_{tot})$ is in the strongest components seen in the trace neutral species] span a somewhat wider range – from $\lesssim$ −3.5 dex (for the main components in moderately reddened sight lines with significant molecular abundances) to $\gtrsim$ −0.3 dex (for some halo components). In general, the titanium depletions become increasingly severe with increasing mean sight line density, total hydrogen column density, or colour excess; the considerable scatter at any given $N(H_{tot})$ or $E(B - V)$ may be due to differences in the proportions of cold, dense gas and warmer, more diffuse gas along the various sight lines. Despite the fairly tight anti-correlation between D(Ti) and $\langle n_H \rangle$, there does not appear to be a clear dependence of the Ti depletion on the local hydrogen density (as determined from C I fine-structure excitation or C_2 rotational excitation) – at least for the relatively small sample of sight lines with estimates for both D(Ti) and n_H currently available. The titanium depletion is roughly constant, at about −1.8 dex (with much scatter) for molecular fractions less than 0.1, but becomes increasingly severe for $f(H_2) \gtrsim 0.1$; some sight lines with $f(H_2) > 0.5$ have D(Ti) < −3.0 dex. Some apparent regional differences in D(Ti) are seen; many of the stars in the Sco-Oph region, for example, exhibit somewhat more severe depletions than are found for most other Galactic sight lines with comparable $N(H_{tot})$, $E(B - V)$, or $f(H_2)$.

While the deuterium depletion hypothesis appears to provide a reasonable explanation for the range in D I/H I ratios observed in the local Galactic ISM, other factors – such as the presence of ionized gas, complex component structures and differences in the severity of the depletions of different elements – may conspire to obscure the expected correlations between the D I/H I ratio and the depletions of various other elements. Additional data for both Ti II and other depleted species, in sight lines where D I has been measured, would

be valuable to better understand those other factors – and thus to better understand the current Galactic D/H ratio.

While the titanium depletions in the Magellanic Clouds exhibit very similar trends with total hydrogen column density, colour excess and molecular fraction to those seen in our Galaxy, the depletions generally are much less severe in the LMC and (especially) the SMC. For a given $N(H_{tot})$, for example, D(Ti) is less severe (on average) by factors of ∼5 in the LMC and ∼20 in the SMC, relative to the mean Galactic value. In the current Magellanic Clouds sample, D(Ti) ranges from about −1.1 to −2.1 dex in the LMC and from about −0.8 to −1.7 dex in the SMC. As in our Galaxy, a somewhat broader range is found for D(Ti) in individual components (for the three Magellanic Clouds sight lines with moderately high resolution spectra of both Ti II and Zn II); some individual components do exhibit fairly severe Ti depletions. Very mild Ti depletions, ranging from −0.5 to −0.1 dex, are found for the 'intermediate-velocity' ($100\,km\,s^{-1} \lesssim v \lesssim 200\,km\,s^{-1}$) gas seen towards several LMC targets.

While some of the differences in average D(Ti) may be due to sampling larger fractions of warmer, more diffuse gas in the LMC and SMC, even the Magellanic Clouds sight lines with strong absorption from Na I and H_2 (and, in several cases, absorption from CN and/or CO) – which presumably probe appreciable amounts of colder, denser gas – exhibit milder Ti depletions than those found for comparable Galactic sight lines. For example, the most severe Ti depletions in the Magellanic Clouds are found towards Sk 143 (SMC) and Sk−67 2 (LMC) – two moderately reddened sight lines with the highest molecular fractions and sole detections of CN absorption in the current sample – but even there the depletions still are much less severe than those in Galactic sight lines with similar $N(H_{tot})$ or $f(H_2)$. The local hydrogen densities in diffuse, neutral clouds in the Magellanic Clouds may be somewhat higher (on average) than those in the local Galactic ISM, so the milder Ti II depletions in the Magellanic Clouds are not due to lower n_H there.

Several of the main components towards Sk 155 (SMC) previously noted to have anomalously mild depletions of Mg and Si also exhibit much less severe Ti depletions than would have been expected from the depletions of Cr, Mn, Fe and Ni in those components. The main components towards Sk−70 115 (LMC), also with somewhat milder than expected depletions of Mg and Si, have very severe Ti depletions, however – consistent with the severe depletions seen for Fe and Ni. High-resolution UV spectra of additional SMC and LMC stars – including the absorption lines from dominant ions of both severely and mildly depleted elements – are needed to better understand the differences in depletion behaviour seen for Mg, Si and Ti in the Magellanic Clouds.

Although Ti II has been detected in relatively few QSO absorption-line systems (DLAs and sub-DLAs), comparisons with corresponding column density data for H I, Ca II and Zn II suggest some similarities in the Ti depletion behaviour to that in the Magellanic Clouds. Like the LMC and SMC sight lines, most (though not all) of the absorbers exhibit somewhat higher Ti II/Ca II ratios than those found for most Galactic sight lines. And while there is considerable scatter in D(Ti) (as gauged from [Ti/Zn]) at any given $N(H_{tot})$ or metallicity, the Ti depletions in the absorbers are (on average) even less severe than those in the LMC and SMC – perhaps indicative of an even higher fraction of warm, diffuse gas in the absorbers. The Ti depletions found for some metal-rich sub-DLAs, however, are similar to those found for Galactic sight lines with comparable $N(H_{tot})$. In (only) apparent contrast to the trends seen within the Milky Way, LMC and SMC, the ensemble of absorber Ti II data exhibits generally milder Ti depletion at higher $N(H_{tot})$ – a consequence of trends for lower metallicities at higher $N(H_{tot})$ and less severe depletions at lower metallicities. As LMC- or SMC-like UV extinction has been inferred for DLAs and sub-DLAs, and as differences in the depletions of Mg, Si and Ti have been noted in at least some LMC and SMC sight lines, the use of Galactic depletion patterns to interpret the gas-phase abundances in the QSO absorbers may not be entirely reliable.

REFERENCES

Albert C. E., 1983, ApJ, 272, 509
Albert C. E., Blades J. C., Morton D. C., Lockman F. J., Proulx M., Ferrarese L., 1993, ApJS, 88, 81
Albert C. E., Welsh B. Y., Danly L., 1994, ApJ, 437, 204
Allen M. M., Jenkins E. B., Snow T. P., 1992, ApJS, 83, 261
André M. K. et al., 2004, A&A, 422, 483
Ardeberg A., Maurice E., 1977, A&AS, 30, 261
Ardeberg A., Brunet J.-P., Maurice E., Prévot L., 1972, A&AS, 6, 249
Azzopardi M., Vigneau J., Macquet M., 1975, A&AS, 22, 285
Ballester P., Modigliani A., Boitquin O., Cristiani S., Hanuschik R., Kaufer A., Wolf S., 2000, Messenger, 101, 31
Blauuw A., 1963, in Strand K. Aa., ed., Stars and Stellar Systems, Vol. 3, Basic Astronomical Data. Univ. Chicago Press, Chicago, p. 401
Bluhm H., de Boer K. S., 2001, A&A, 379, 82
Bohlin R. C., Savage B. D., Drake J. F., 1978, ApJ, 224, 132
Bouchet P., Lequeux J., Maurice E., Prevot L., Prevot-Burnichon M. L., 1985, A&A, 149, 330
Brunet J. P., Imbert M., Martin N., Mianes P., Prévot L., Rebeirot E., Rousseau J., 1975, A&AS, 21, 109
Cartledge S. I. B. et al., 2005, ApJ, 630, 355
Caulet A., Newell R., 1996, ApJ, 465, 205
Cha A. N., Sembach K. R., 2000, ApJ, 126, 399
Chaffee F. C., 1974, ApJ, 189, 427
Chaffee F. C., Dunham T., 1979, ApJ, 233, 568
Chaffee F. C., Lutz B. L., 1977, ApJ, 213, 394
Cox N. L. J., Cordiner M. A., Cami J., Foing B. H., Sarre P. J., Kaper L., Ehrenfreund P., 2006, A&A, 447, 991
Cox N. L. J. et al., 2007, A&A, 470, 941
Crawford I. A., 1995, MNRAS, 277, 458
Crawford I. A., 2003, Ap&SS, 285, 661
Crawford I. A., Barlow M. J., Diego F., Spyromilio J., 1994, MNRAS, 266, 903
Crinklaw G., Federman S. R., Joseph C. L., 1994, ApJ, 424, 748
Crowther P. A., 2007, ARA&A, 45, 177
Crowther P. A., Dessart L., 1998, MNRAS, 296, 622
Crowther P. A., Smith L. J., 1997, A&A, 320, 500
Crowther P. A., Hillier D. J., Evans C. J., Fullerton A. W., De Marco O., Willis A. J., 2002, ApJ, 579, 774
Cui J., Bechtold J., Ge J., Meyer D. M., 2005, ApJ, 633, 649

Dachs J., 1970, A&A, 9, 95

Danforth C., Howk J. C., Fullerton A. W., Blair W. P., Sembach K. R., 2002, ApJS, 139, 81

Danks A. C., Walborn N. R., Vieira G., Landsman W. B., Gales J., García B., 2001, ApJ, 547, L155

de Boer K. S., Morras R., Bajaja E., 1990, A&A, 233, 523

de la Varga A., Reimers D., Tytler D., Barlow T., Burles S., 2000, A&A, 363, 69

Dekker H., D'Odorico S., Kaufer A., Delabre B., Kotzlowski H., 2000, Proc. SPIE, 4008, 534

Dessauges-Zavadsky M., Calura F., Prochaska J. X., D'Odorico S., Matteucci F., 2004, A&A, 416, 79

Dessauges-Zavadsky M., Ellison S. L., Murphy M. T., 2009, MNRAS, 396, L61

Dessauges-Zavadsky M., Prochaska J. X., D'Odorico S. D., 2002, A&A, 391, 801

Dessauges-Zavadsky M., Prochaska J. X., D'Odorico S., Calura F., Matteucci F., 2006, A&A, 445, 93

Diplas A., Savage B. D., 1994, ApJ, 427, 284

Draine B. T., 2006, in Sonneborn G., Moos H. W., Andersson B.-G., eds, ASP Conf. Ser. Vol. 348, Astrophysics in the Far Ultraviolet: Five Years of Discovery with FUSE, Astron. Soc. Pac., San Francisco, p. 58

Dunkin S. K., Crawford I. A., 1999, MNRAS, 302, 197

Edgar R. J., Savage B. D., 1989, ApJ, 340, 762

Ellison S. L., Prochaska J. X., Lopez S., 2007, MNRAS, 380, 1245

Evans C. J., Crowther P. A., Fullerton A. W., Hillier D. J., 2004, ApJ, 610, 1021

Federman S. R., Weber J., Lambert D. L., 1996, ApJ, 463, 181

Fehrenbach C., Duflot M., 1982, A&AS, 48, 409

Feitzinger J. V., Isserstedt J., 1983, A&AS, 51, 505

Felenbok P., Roueff E., 1996, ApJ, 465, L57

FitzGerald M. P., 1970, A&A, 4, 234

Fitzpatrick E. L., 1985a, ApJS, 59, 77

Fitzpatrick E. L., 1985b, ApJ, 299, 219

Fitzpatrick E. L., 1986, AJ, 92, 1068

Fitzpatrick E. L., 1988, ApJ, 335, 703

Fitzpatrick E. L., 1991, PASP, 103, 1123

Fitzpatrick E. L., Massa D., 1990, ApJS, 72, 163

Fitzpatrick E. L., Spitzer L., 1997, ApJ, 475, 623

Garmany C. D., Conti P. S., Massey P., 1987, AJ, 93, 1070

Gonzalez G., Wallerstein G., 1999, AJ, 117, 2286

Gordon K. D., Clayton G. C., Misselt K. A., Landolt A. U., Wolff M. J., 2003, ApJ, 594, 279

Gredel R., van Dishoeck E. F., Black J. H., 1991, A&A, 251, 625

Herbert-Fort S., Prochaska J. X., Dessauges-Zavadsky M., Ellison S. L., Howk J. C., Wolfe A. M., Prochter G. E., 2006, PASP, 118, 1077

Herbig G. H., 1993, ApJ, 407, 142

Hill V., 1997, A&A, 324, 435

Hill V., 1999, A&A, 345, 430

Hill V., Andrievsky S., Spite M., 1995, A&A, 293, 347

Hobbs L. M., 1974, ApJ, 191, 381

Hobbs L. M., 1979, ApJ, 229, L129

Hobbs L. M., 1983, ApJ, 265, 816

Hobbs L. M., 1984, ApJS, 56, 315

Hobbs L. M., Ferlet R., Welty D. E., Wallerstein G., 1991, ApJ, 378, 586

Howk J. C., Savage B. D., Fabian D., 1999, ApJ, 525, 253

Hunter I., Smoker J. V., Keenan F. P., Ledoux C., Jehin E., Cabanac R., Melo C., Bagnulo S., 2006, MNRAS, 367, 1478

Isserstedt J., 1975, A&AS, 19, 259

Isserstedt J., 1979, A&AS, 38, 329

Isserstedt J., 1982, A&AS, 50, 7

Jenkins E. B., 1987, in Hollenbach D. J., Thronson H. A., eds, Interstellar Processes. Reidel, Dordrecht, p. 533

Jenkins E. B., 1996, ApJ, 471, 292

Jenkins E. B., 2004, in McWilliam A., Rauch M., eds, Carnegie Obs. Centennial Symp., Origin and Evolution of the Elements. Cambridge Univ. Press, Cambridge, p. 336

Jenkins E. B., 2009, ApJ, 700, 1299

Jenkins E. B., Tripp T. M., 2001, ApJS, 137, 297

Jenkins E. B., Drake J. F., Morton D. C., Rogerson J. B., York D. G., 1973, ApJ, 181, L122

Jenkins E. B., Savage B. D., Spitzer L., 1986, ApJ, 301, 355

Jensen A. G., Snow T. P., 2007, ApJ, 669, 378

Johnson H. L., 1963, in Strand K. Aa., ed., Stars and Stellar Systems, Vol. 3, Basic Astronomical Data. Univ. Chicago Press, Chicago, p. 214

Jorgenson R. A., Wolfe A. M., Prochaska J. X., Carswell R. F., 2009, ApJ, 704, 247

Joseph C. L., Jenkins E. B., 1991, ApJ, 368, 201

Jura M., 1982, in Kondo Y., Mead J. M., Chapman R. D., eds, NASA Conf. Publ. 2238, Advances in UV Astronomy: 4 Years of IUE Research. NASA, Greenbelt, p. 54

Kanekar N., Smette A., Briggs F. H., Chengalur J. N., 2009, ApJ, 705, L40

Khare P., Kulkarni V. P., Lauroesch J. T., York D. G., Crotts A. P. S., Nakamura O., 2004, ApJ, 616, 86c

Khare P., Kulkarni V. P., Péroux C., York D. G., Lauroesch J. T., Meiring J. D., 2007, A&A, 464, 487

Kulkarni V. P., Fall S. M., Lauroesch J. T., York D. G., Welty D. E., Khare P., Truran J. W., 2005, ApJ, 618, 67

Kulkarni V. P., Khare P., Péroux C., York D. G., Lauroesch J. T., Meiring J. D., 2007, ApJ, 661, 88

Lallement R., Hébrard G., Welsh B. Y., 2008, A&A, 481, 381

Lauroesch J. T., 2007, in Haverkorn M., Goss W. M., eds, ASP Conf. Ser. Vol. 365, SINS – Small Ionized and Neutral Structures in the Diffuse Interstellar Medium. Astron. Soc. Pac., San Francisco, p. 40

Lauroesch J. T., Truran J. W., Welty D. E., York D. G., 1996, PASP, 108, 641

Ledoux C., Bergeron J., Petitjean P., 2002, A&A, 385, 802

Ledoux C., Petitjean P., Srianand R., 2003, MNRAS, 346, 209

Lehner N., Staveley-Smith L., Howk J. C., 2009, ApJ, 702, 940

Lennon D. J., 1997, A&A, 317, 871

Levshakov S. A., Dessauges-Zavadsky M., D'Odorico S., Molaro P., 2002, ApJ, 565, 696

Li A., Misselt K. A., Wang Y. J., 2006, ApJ, 640, L151

Linsky J. L., 2009, in Van Steenberg M., Sonneborn G., Moos H. W., Blair W. P., eds, AIP Conf. Proc. Vol. 1135, Future Directions in Ultraviolet Spectroscopy. Springer-Verlag, Berlin, p. 63

Linsky J. L. et al., 2006, ApJ, 647, 1106

Lipman K., Pettini M., 1995, ApJ, 442, 628

Lodders K., 2003, ApJ, 591, 1220

Lu L., Sargent W. L. W., Barlow T. A., Churchill C. W., Vogt S. S., 1996, ApJS, 107, 475

Luck R. E., Lambert D. L., 1992, ApJS, 79, 303

Luck R. E., Moffett T. J., Barnes T. G., Gieren W. P., 1998, AJ, 115, 605

Magnani L., Salzer J., 1989, AJ, 98, 926

Magnani L., Salzer J., 1991, AJ, 101, 1427

Massey P., 2002, ApJS, 141, 81

Massey P., Lang C. C., DeGioia-Eastwood K., Garmany C. D., 1995, ApJ, 438, 188

Massey P., Puls J., Pauldrach A. W. A., Bresolin F., Kudritzki R. P., Simon T., 2005, ApJ, 627, 477

Maurice E., Bouchet P., Martin N., 1989, A&AS, 78, 445

McCall B. J. et al., 2002, ApJ, 567, 391

Meiring J. D., 2009, PhD thesis, Univ. South Carolina

Meiring J. D. et al., 2006, MNRAS, 370, 43

Meiring J. D., Kulkarni V. P., Lauroesch J. T., Péroux C., Khare P., York D. G., Crotts A. P. S., 2008, MNRAS, 384, 1015

Meiring J. D., Kulkarni V. P., Lauroesch J. T., Péroux C., Khare P., York D. G., 2009, MNRAS, 393, 1513

Meyer D. M., Roth K. C., 1991, ApJ, 376, L49

Miller A., Lauroesch J. T., Sofia U. J., Cartledge S. I. B., Meyer D. M., 2007, ApJ, 659, 441

Morton D. C., 2003, ApJS, 149, 205

Nestor D. B., Pettini M., Hewett P. C., Rao S., Wild V., 2008, MNRAS, 390, 1670

Noterdaeme P., Ledoux C., Petitjean P., Le Petit F., Srianand R., Smette A., 2007, A&A, 474, 393

Noterdaeme P., Ledoux C., Petitjean P., Srianand R., 2008, A&A, 481, 327

Palmer B. A., Engelman R., 1983, Atlas of the Thorium Spectrum. Los Alamos Natl. Lab., Los Alamos, NM

Pan K., Federman S. R., Cunha K., Smith V. V., Welty D. E., 2004, ApJS, 151, 313

Parker J. Wm., 1993, AJ, 106, 560

Pei Y. C., Fall S. M., Bechtold J., 1991, ApJ, 378, 6

Penprase B. E., 1993, ApJS, 88, 433

Péroux C., Kulkarni V. P., Meiring J. D., Ferlet R., Khare P., Lauroesch J. T., Vladilo G., York D. G., 2006a, A&A, 450, 53

Péroux C., Meiring J. D., Kulkarni V. P., Ferlet R., Khare P., Lauroesch J. T., Vladilo G., York D. G., 2006b, MNRAS, 372, 369

Péroux C., Meiring J. D., Kulkarni V. P., Khare P., Lauroesch J. T., Vladilo G., York D. G., 2008, MNRAS, 386, 2209

Pettini M., 2006, in Sonneborn G., Moos H. W., Andersson B.-G., eds, ASP Conf. Ser. Vol. 348, Astrophysics in the Far Ultraviolet: Five Years of Discovery with FUSE. Astron. Soc. Pac., San Francisco, p. 19

Pettini M., Gillingham P., 1988, AAO Newsletter 43

Pettini M., Zych B. J., Murphy M. T., Lewis A., Steidel C. C., 2008, MNRAS, 391, 1499

Price R. J., Crawford I. A., Barlow M. J., Howarth I. D., 2001, MNRAS, 328, 555

Prochaska J. X., Wolfe A. M., 2002, ApJ, 566, 68

Prochaska J. X. et al., 2001, ApJS, 137, 21

Prochaska J. X., Gawiser E., Wolfe A. M., Cooke J., Gelino D., 2003a, ApJS, 147, 227

Prochaska J. X., Gawiser E., Wolfe A. M., Castro S., Djorgovski S. G., 2003b, ApJ, 595, L9

Prochaska J. X., Tripp T. M., Howk J. C., 2005, ApJ, 620, L39

Prochaska J. X., Wolfe A. M., Howk J. C., Gawiser E., Burles S. M., Cooke J., 2007, ApJS, 171, 29

Quast R., Reimers D., Baade R., 2008, A&A, 477, 443

Rachford B. L. et al., 2009, ApJS, 180, 125

Rachford B. L. et al., 2001, ApJ, 555, 839

Rachford B. L. et al., 2002, ApJ, 577, 221

Reimers D., Baade R., Quast R., Levshakov S. A., 2003, A&A, 410, 785

Roth K. C., Blades J. C., Albert C. E., 1995, AAS Meeting 186, 35.02

Russell S. C., Bessell M. S., 1989, ApJS, 70, 865

Russell S. C., Dopita M. A., 1992, ApJ, 384, 508

Savage B. D., de Boer K. S., 1981, ApJ, 243, 460

Savage B. D., Sembach K. R., 1991, ApJ, 379, 245

Savage B. D., Sembach K. R., 1996, ARA&A, 34, 279

Savage B. D., Wakker B. P., 2009, ApJ, 702, 1472

Savage B. D., Bohlin R. C., Drake J. F., Budich W., 1977, ApJ, 216, 291

Savage B. D., Lehner N., Fox A. J., Wakker B. P., Sembach K. R., 2007, ApJ, 659, 1222

Schlegel D. J., Finkbeiner D. P., Davis M., 1998, ApJ, 500, 525

Schmidt-Kaler Th., Gochermann J., Oestreicher M. O., Grothues H.-G., Tappert C., Zaum A., Berghöfer Th., Brugger H. R., 1999, MNRAS, 306, 279

Sembach K. R., Savage B. D., 1992, ApJS, 83, 147

Sembach K. R., Danks A. C., Savage B. D., 1993, A&AS, 100, 107

Sembach K. R. et al., 2004, ApJS, 150, 387

Snow T. P., Black J. H., van Dishoeck E. F., Burks G., Crutcher R. M., Lutz B. L., Hanson M. M., Shuping R. Y., 1996, ApJ, 465, 245

Snow T. P., Rachford B. L., Figoski L., 2002, ApJ, 573, 662

Snow T. P., Destree J. D., Welty D. E., 2008, ApJ, 679, 512

Sofia U. J., Gordon K. G., Clayton G. C., Misselt K., Wolff M. J., Cox N. L. J., Ehrenfreund P., 2006, ApJ, 636, 753

Sonnentrucker P., Welty D. E., Thorburn J. A., York D. G., 2007, ApJS, 168, 58

Spite F., Spite M., Francois P., 1989, A&A, 210, 25

Spite F., Barbuy B., Spite M., 1993, A&A, 272, 116

Spitzer L., 1985, ApJ, 290, L21

Spitzer L., Fitzpatrick E. L., 1993, ApJ, 409, 299

Staveley-Smith L., Kim S., Calabretta M. R., Haynes R. F., Kesteven M. J., 2003, MNRAS, 339, 87

Steigman G., 2009, in Van Steenberg M., Sonneborn G., Moos H. W., Blair W. P., eds, AIP Conf. Proc. Vol. 1135, Future Directions in Ultraviolet Spectroscopy. Springer-Verlag, Berlin, p. 94

Steigman G., Romano D., Tosi M., 2007, MNRAS, 378, 576

Stokes G., 1978, ApJS, 36, 115

Stokes G. M., Hobbs L. M., 1976, ApJ, 208, L95

Thorburn J. A. et al., 2003, ApJ, 584, 339

Tielens A. G. G. M., 1983, A&A, 119, 177

Trundle C., Lennon D. J., 2005, A&A, 434, 677

Tumlinson J. et al., 2002, ApJ, 566, 857

van Dishoeck E. F., Black J. H., 1982, ApJ, 258, 533

Venn K. A., 1999, ApJ, 518, 405

Vladilo G., 2002, A&A, 391, 407

Vladilo G., 2004, A&A, 421, 479

Vladilo G., Prochaska J. X., Wolfe A. M., 2008, A&A, 478, 701

Wakker B. P., Mathis J. S., 2000, ApJ, 544, L107

Walborn N. R., 1977, ApJ, 215, 53

Walborn N. R., Lennon D. J., Haser S. M., Kudritzki R.-P., Voels S. A., 1995, PASP, 107, 104

Walborn N. R., Lennon D. J., Heap S. R., Lindler D. J., Smith L. J., Evans C. J., Parker J. W., 2000, PASP, 112, 1243

Walborn N. R., Danks A. C., Vieira G., Landsman W. B., 2002a, ApJS, 140, 407

Walborn N. R., Fullerton A. W., Crowther P. A., Bianchi L., Hutchings J. B., Pellerin A., Sonneborn G., Willis A. J., 2002b, ApJS, 141, 443

Walborn N. R. et al., 2002c, AJ, 123, 2754

Walborn N. R. et al., 2010, AJ, 139, 1283

Wallerstein G., Gilroy K. K., 1992, AJ, 103, 1346

Wallerstein G., Goldsmith D., 1974, ApJ, 187, 237

Wayte S. R., 1990, ApJ, 355, 473

Welsh B. Y., Sasseen T., Craig N., Jelinsky S., Albert C. E., 1997, ApJS, 112, 507

Welty D. E., 2007, ApJ, 668, 1012

Welty D. E., Federman S. R., Gredel R., Thorburn J. A., Lambert D. L., 2006, ApJS, 165, 138

Welty D. E., Fowler J. R., 1992, ApJ, 393, 193

Welty D. E., Frisch P. C., Sonneborn G., York D. G., 1999a, ApJ, 512, 636

Welty D. E., Hobbs L. M., 2001, ApJS, 133, 345

Welty D. E., Hobbs L. M., Kulkarni V. P., 1994, ApJ, 436, 152

Welty D. E., Hobbs L. M., Lauroesch J. T., Morton D. C., Spitzer L., York D. G., 1999b, ApJS, 124, 465

Welty D. E., Hobbs L. M., Morton D. C., 2003, ApJS, 147, 61

Welty D. E., Lauroesch J. T., Blades J. C., Hobbs L. M., York D. G., 1997, ApJ, 489, 672

Welty D. E., Lauroesch J. T., Blades J. C., Hobbs L. M., York D. G., 2001, ApJ, 554, L79

Welty D. E., Lauroesch J. T., Hobbs L. M., York D. G., 2004, BAAS, 36, 1441

Welty D. E., Morton D. C., Hobbs L. M., 1996, ApJS, 106, 533

Welty D. E., Simon T., Hobbs L. M., 2008, MNRAS, 388, 323

Wild V., Hewett P. C., 2005, MNRAS, 361, 30

Wild V., Hewett P. C., Pettini M., 2006, MNRAS, 367, 211

Wolfire M. G., Hollenbach D., McKee C. F., Tielens A. G. G. M., Bakes E. L. O., 1995, ApJ, 443, 152

Wong T. et al., 2009, ApJ, 696, 370

York D. G., Rogerson J. B., 1976, ApJ, 203, 378

York D. G. et al., 2006, MNRAS, 367, 945

Zhou H., Ge J., Lu H., Wang T., Yuan W., Jiang P., Shan H., 2010, ApJ, 708, 742

Zsargó J., Federman S. R., 2003, ApJ, 589, 319

Zych B. J., Murphy M. T., Hewett P. C., Prochaska J. X., 2009, MNRAS, 392, 1429

SUPPORTING INFORMATION

Additional Supporting Information may be found in the online version of this article:

Appendix A. Spectra, equivalent widths and column densities.

Please note: Wiley-Blackwell are not responsible for the content or functionality of any supporting materials supplied by the authors. Any queries (other than missing material) should be directed to the corresponding author for the article.

This paper has been typeset from a TEX/LATEX file prepared by the author.